This is the accepted version with minor changes of: Carlos A. Morales Rodriguez, Joan Montanyà, Oscar A. van der Velde, Ferran Fabró, Jesus A. Lopez (2021), Tropical TGF Paradox: A Perspective From TRMM Precipitation Radar, Journal of Geophysical Research Atmospheres, https://doi.org/10.1029/2021JD034698

Tropical TGF Paradox: A Perspective From TRMM Precipitation Radar

Carlos A. Morales Rodriguez[1], Joan Montanyà[2], Oscar A. van der Velde[2], Ferran Fabró[3], Jesus A. Lopez[2]

[1]Departamento de Ciências Atmosféricas, Instituto de Astronomia, Geofísica e Ciências Atmosféricas, Universidade de São Paulo, São Paulo, Brazil

[2]Polytechnic University of Catalonia, Terrassa, Spain

[3]Meteorological Service of Catalonia, Barcelona, Spain

Corresponding Author: carlos.morales@iag.usp.br

Key Points:

- TGF related thunderstorms present bimodal precipitation distributions above -20^{o}C while the Climatology shows a unimodal distribution.
- TGF thunderstorms, in relation to the Climatology thunderstorms, have greater distance between the electrical opposite charging layers.
- African TGF thunderstorms have more positive charges close to the negative charging layer.

Abstract

The Terrestrial Gamma-ray Flash (TGF) to lightning ratio, computed over the 3 tropical chimneys, presents a paradox: African thunderstorms produce the most lightning but yield the lowest fraction of TGFs when compared to American and Southeast Asian thunderstorms. To understand the physical insights into this asymmetry, TRMM Precipitation Radar measurements are used to depict the vertical precipitation structure and infer the vertical electrical charge fraction distribution of the observed thunderstorms in the 3 regions and the thunderstorms during TGF occurrences detected by the AGILE, Fermi-GBM and RHESSI sensors. Regional differences show that African thunderstorms are taller, smaller, and have a higher concentration of dense ice particles above the freezing level in addition to having more lightning flashes per thunderstorm. The overall TGF related thunderstorms are taller, more intense (0.5-1.5 dBZ) and present similar radar reflectivity decay with height independent of the region. The two dimensional precipitation vertical distribution diagrams indicate bimodal distribution above -20^{o}C for TGF thunderstorms (developing stage characteristic), while the overall thunderstorm population, here defined as Climatology, showed a unimodal distribution (mature phase). Independent of the region, thunderstorms show a midlevel negative charge center varying from 4.6 to 8.1 km in height and an upper level positive charge center ranging from 7.4 to 14.6 km. TGF thunderstorms have thicker positive charging layer and present larger vertical distances between the opposite charging layers in comparison with the Climatology. African TGF thunderstorms have higher fraction of positive charges near the negative layer, helping to produce more and shorter lightning discharges.

Plain Language Summary

Terrestrial Gamma-ray Flashes (TGFs) have been detected in space above thunderstorms worldwide, but their main triggering mechanism has not yet been fully understood. In the last two decades, several measurements from ground and satellite instruments have provided information to help our understanding. For instance, TGF emissions are concentrated in the tropics and one of possible theories suggests to be related to intense intra-cloud lightning processes produced by thunderstorms that have considerable vertical charge center separations. Although African thunderstorms have the highest lightning activity in the world, they produce fewer TGFs per number of lightning flashes than thunderstorms in America and the Southeast Asia tropical regions, posing a paradox. To explore this asymmetry, this study employed 3D measurements from the Precipitation Radar on board the Tropical Rainfall Measuring Mission (TRMM) satellite to describe the main precipitation vertical structure observed in the 3 most important tropical thunderstorm regions in the world (Climatology) and in the thunderstorms that produced TGFs. African thunderstorms are taller and smaller, in addition to having more ice aloft and lightning discharges. The TGF-producing thunderstorms, however, show similar precipitation variation decay with height independent of the region, in addition to being taller, slightly more intense, having a different vertical cloud charge structure and a larger distance between the opposite charge layers.

1 Introduction

Almost 20 years since the discovery of Terrestrial Gamma-ray Flashes (TGFs) by *Fishman et al.* (1994), the environment of the source of these sub-millisecond pulse-like emissions of MeV energetic gamma ray photons (*Briggs et al.,* 2010; *Marisaldi et al.,* 2019 and *Østgaard et al.*, 2019) is still not well understood. It is accepted that these emissions are related to intra-cloud lightning processes (e.g. *Cummer et al.,* 2005 and 2015), and the identification of those thunderstorms that lead to the production of TGFs is a subject of great interest (e.g. *Fabró et al.*, 2019).

In the last decade, up to 2014, several space-based missions (e.g. Burst and Transient Source Experiment – BATSE [*Fishman et al.*, 1994], Reuven Ramaty High Energy Solar Spectroscopic Imager - RHESSI [*Smith et al.* 2005], Astrorivelatore Gamma a Immagini Leggero - AGILE [*Marisaldi et al.*, 2010], Fermi Gamma-ray Burst Monitor - Fermi-GBM [*Briggs et al.,* 2010] and Atmosphere-Space Interactions Monitor – ASIM [*Østgaard et al*., 2019]) observed 5,420 TGFs worldwide (Figure 1), which revealed an asymmetric behavior between the 3 tropical "chimneys" (America, Africa and Southeast Asia). Namely, the most prolific lightning producer, the African continent, produces fewer TGFs per flash rate than the American and Southeast Asian regions (*Smith et al.* 2010, *Splitt et al. 2011*, *Fuschino et al.* 2011, *Briggs et al.* 2013, *Fabró et al.* 2019). This last study proposed that the higher intra-cloud (IC) flash rates observed in the African thunderstorms may explain this paradox if these thunderstorms present shorter distances between the main opposite polarity electrical charge centers, in addition to having higher altitude charge layers when compared to American and Southeast Asian thunderstorms. Consequently, African thunderstorms provide convenient conditions for high IC flash rates, which result in IC discharges with shorter horizontal/vertical extension, less energy and shorter time duration in contrast to the more energetic lightning flashes observed with TGF (*Cummer et al*., 2015, *Smith et al*., 2018), and a longer time interval between the strokes just prior to the TGF occurrence (*Larkey et al*., 2019). These features might be an effect of the partitioning of water and ice particles that control the electrification processes within thunderstorms (*Saunders et al*., 2006). For instance, *Barnes et al.* (2015) found more ice and water particles (cloud and precipitating) in TGF related thunderstorms than non-TGF storms. With a different methodology, *Ursi et al.* (2019) found ice phase clouds related to TGF thunderstorms which had large ice particles at higher levels.

To evaluate the relationship between thunderstorms in the tropical chimney regions and TGF production and its association with the precipitation vertical structure that control the electrification processes, the following two questions will be addressed: Does the vertical distance between the electrical charge centers dictate the production of TGF? Does the vertical structure of thunderstorms explain the TGF to lightning flash rate asymmetry observed in the 3 chimneys?

2 Methodology and Data

As mention in the introduction, this study seeks to improve the understanding of the observed TGF to lightning flash rate asymmetry observed in the 3 tropical lightning chimneys, i.e., America (90-70W & 0-20N), Africa (15-35E & 10S-10N), and Southeast Asia 95-115E & 10S-10N). The definition of these regions is based on the study of

Fabró et al (2019) that identified the areas with maximum TGF activity as illustrated in Figure 1. Along the year, the weather patterns in each of these three regions do not change considerably to produce different types of thunderstorms. Thus, seasonal variations would not affect the mean characterization of the observed thunderstorms because the acting precipitating and convective systems are almost de same [for more detailed information about the meteorological weather systems acting in these 3 regions see *Philander*, 1989].

To understand and explore the cloud microphysical properties observed in this TGF paradox and seek physical explanations, this study uses measurements from the Precipitation Radar (PR) (*Iguchi et al.,* 2000) and Lightning Imaging Sensor (LIS) (*Christian et al.,* 1999) on board the Tropical Rainfall Measuring Mission (TRMM) satellite (*Kummerow et al.,* 1998) to initially characterize the main vertical precipitation structure observed in all scanned thunderstorms of the 3 tropical chimneys (Table 1). As these precipitation features represent the overall characteristic for each region, we refer to this climatological data population as the Climatology. Secondly, the AGILE, Fermi-GBM and RHESSI TGF subsatellite point locations with coincident TRMM PR measurements are used to evaluate the mean vertical precipitation structure of thunderstorms associated with the occurrence of TGFs in each chimney, and for simplicity they will be denoted as TGF thunderstorms. Lastly, the vertical precipitation profiles (Climatology and TGF) are augmented to infer the thunderstorm electrical charge distributions based on the non-inductive process (Takahashi, 1978) to diagnose how the charge layer separation contributes to the development of TGFs.

Table 1. Number of TRMM orbits and the respective number of thunderstorms observed in each tropical chimney during the 1998-2014 period and the number of TRMM orbits associated with TGFs detected by the AGILE, Fermi-GBM and RHESSI satellite missions during their period of observation.

	TRMM		
Region	Orbits	Thunderstorms	Number of Orbits with coincident TGF
America (90-70W & 0-20N)	3,690	11,391	35
Africa (15-35E & 10S-10N)	4,089	23,656	43
SE Asia (95-115E & 10S-10N)	1,993	6,117	46

2.1 Precipitation Vertical Structure

A total of 9,772 TRMM-PR and LIS orbits observed during the period between 1998 and 2014 have been employed to compute the mean thunderstorm vertical structure observed in the 3 chimney regions (America, African and SE Asia) with maximum TGF activity defined by areas of 20 x 20 degrees (Table 1), Figure 1.

For this study, thunderstorms are defined as contiguous rain area with more than 2 TRMM PR pixels (~ a footprint size of 5 x 5 km^2 with 250 m vertical resolution) with at least one LIS lightning flash within the field of view (*Morales Rodriguez*, 2019). Moreover, only TRMM-PR convective rain type profiles (*Awaka et al*., 1997) are used in the analysis since more than 90% of the lightning flashes fall into the convective rain category and where it is expected to have significant vertical velocities. In these convective cores, the accretion process predominates and leads to the formation of graupel and hail. These particles are essential hydrometeor ingredients for the non-inductive electrification mechanism (*Takahashi*, 1978, *Saunders et al.,* 2006). Based on this procedure, a total of 41,164 thunderstorms have been identified in the TRMM orbits over the 3 tropical chimney regions, Table 1.

The 3D precipitation structure is based on the mean vertical profile of radar reflectivity factor (Z) with 1 km vertical resolution. Z is proportional to the diameter of the particle to the power of six multiplied by the particle size concentration ($Z_e[\frac{mm^6}{m^3}] = \int_0^\infty N(D)D^6dD$) (*Battan*, 1973), and it is expressed in decibels of Z (dBZ) ($Z[dBZ] = 10log_{10}Z_e\left[\frac{mm^6}{m^3}\right]$). Therefore, to evaluate the mean radar reflectivity value it is necessary to linearize Z to mm^6/m^3 ($Z_e\left[\frac{mm^6}{m^3}\right] = 10^{\frac{Z[dBZ]}{10}}$) first. Then, we compute the mean Z_e value for each vertical layer and convert back to dBZ. The profiles are computed from surface up to 20 km with 1 km altitude resolution. Furthermore, the altitude levels are also converted to air temperature by means of the NOAA National Center for Environmental Prediction (NCEP) and the National Center of Atmospheric Research (NCAR) reanalysis (Reanalysis-1) (*Kalnay et al.*, 1996). Basically, TRMM PR heights are transformed into air temperature by employing the vertical air temperature and geopotential height observed in the location and date of TRMM overpasses using the same procedure shown by *Morales Rodriguez* (2019). By using temperature profiles instead of height it is possible to explore the mechanisms of microphysical growth and electrification between the isotherms of 0 and -40°C. The corresponding radar reflectivity profiles as a function of temperature are presented in Appendix A.

To complement the 3D precipitation structure analysis, two-dimensional histogram distributions of radar reflectivity with height, known as contoured frequency altitude distributions (CFAD) after *Yuter and Houze Jr* (1995) and temperature (CFTD) are computed. The radar reflectivity distributions are binned with an interval of 1 dBZ every 1 km vertical resolution. For the CFTD, the temperature vertical resolution value corresponds to the mean temperature of all profiles in each 1 km binned layer. These diagrams help to interpret the mean vertical profile by complementing the mean and standard deviation values retrieved. Secondly, they provide a better understanding of the hydrometeor growth mechanisms active in the cloud and its relation with the life cycle stage (*Yuter and Houze Jr, 1995*). Additionally, they show how the partitioning of water and ice particles is changing above the freezing level. Lastly, to illustrate how different the radar reflectivity distributions with height and temperature are, the CFAD or CFTD differences will be computed between the regions and against Climatology and TGF thunderstorms of the same chimney. Such representations show the relative frequency difference between two probability distributions and help to interpret how strong/weak those thunderstorms in respect to each other are. The CFADs are shown in the manuscript while the correspondent CFTD will be shown in the Appendix B.

Finally, the 30 dBZ echo-top height and temperature, in addition to the variation of Z with altitude (dZ/dh) or temperature (dZ/dT) are computed for each extracted thunderstorm. The 30 dBZ echo-top is correlated with the lightning activity and the convection strength (*Liu et al.*, 2012) and can be used to explain the differences between the lightning activity in each chimney. The vertical Z gradient can be used to explain how cloud droplets, rain drops and ice particles grow in the thunderstorm, in addition to identifying which growth mechanism is active or predominating *(Rosenfeld and Ulbrich*, 2003; *Yuter and Ho*uze *Jr*, 1995).

2.2 Thunderstorms associated with TGF

To infer the vertical precipitation structure of thunderstorms that are associated with TGF observations, we extracted thunderstorms from TRMM PR and LIS measurements that are close in space and time to TGF observations of the AGILE (2009-03-02 to 2012-07-30), Fermi-GBM (2008-08-07 to 2014-12-31), and RHESSI (2002-03-04 to 2010-09-06) using a methodology similar to *Barnes et al.* (2015).

Basically, as the AGILE, Fermi-GBM and RHESI missions could not detect the precise TGF location, and simultaneous TRMM overpasses are unlikely due to the different orbital characteristics of the all above satellites, we seek the nearest active thunderstorm, an approach similar to *Barnes et al.* (2015), who used the TRMM Microwave Imager (TMI) overpasses within ± 1 hour and up to 500 km from the RHESSI TGF reported locations to characterize the microphysical properties of the TGF and non-TGF storms. For this study, though, we are more time conservative and select the closest thunderstorm observed by TRMM-PR and LIS within +/- 30 minutes of the TGF detection and up to 600 km from the TGF triggered location (subsatellite points of AGILE, Fermi-GBM and RHESSI) provided. By doing this, while unrelated storms are also included within these criteria, we are assuming that this method may capture a signal of the closest microphysical characteristics observed during the lifecycle of TGF related storms.

Based on this approach, it was possible to identify 124 TRMM coincident orbits with active thunderstorms that had coincident TGF observations from AGILE, Fermi-GBM or RHESSI satellite missions that met the distance and time criteria defined before, listed in Table 1. (A detailed description of the TGF occurrence and correspondent TRMM matches is presented in Appendix C). In terms of the continental regions, 35 orbits with active thunderstorms were found in America, 43 in Africa and 46 in SE Asia, Table 1. Note that Africa has the lowest number of detected TGF compared to the number of observed thunderstorms.

2.3 Electrical charge structure

To infer the vertical electric charge structure observed in the extracted thunderstorms, we employed the Takahashi (1978) study that experimentally retrieved the charge gained by graupel during the collision with ice particles growing in an environment with super cooled water droplets. In this approach, the polarity and charge gained by the ice particles is a function of liquid water content (LWC) and air temperature. In this way, we need to convert the vertical profiles of radar reflectivity into profiles of liquid water content as a function of temperature. For this conversion we employed Musunaga et al. (2002) work that derived LWC-Z relationships based on TRMM-PR 2A25 drop size distribution model (Iguchi et al.,2000). Therefore, we could label "TRMM-PR LWC product". The equations are dependent on the height of 0^oC isotherm and precipitation type, i.e., convective, stratiform or others. For this, we use only convective rain type profiles and the charge transfer is limited to the altitudes above the freezing level. As a result we inferred the LWC profiles using the following equations:

For altitude levels with temperature lower than 0^oC and 750 m above the freezing level:

$$LWC(g/m3) = 0.006Z_e^{0.689}$$

For altitude levels within ± 750 m of the freezing level ($T=0^oC$),

$$LWC(g/m3) = 0.003Z_e^{0.578}$$

where Z_e is in mm^6/m^3.

For each thunderstorm we compute the vertical profiles of positive and negative charges gained based on the vertical profiles of temperature and liquid water content using Takahashi (1978) results. Basically, for each LWC and temperature pair at temperatures below 0 ^oC, we check if the charge gained is either positive or negative and assign a value of +1 and -1 respectively. As a result, for each thunderstorm we have several correspondent charge gained profiles that have +1 or -1 every level below the isotherm of 0^oC. Next, for each thunderstorm we create two profiles with 1 km vertical resolution, i.e., one for positive charges and the other for negative charges. Next, we count the number of times that each altitude level has been assigned with +1 (positive charges profile) and -1 (negative charges profile) value and store in the respective polarity profile. Then, we normalize these positive and negative vertical profiles in respect to the total number of charges gained for each polarity. Lastly we compute the respective charge fraction for each polarity, which will represent a total of 50% fraction for each polarity. Therefore, for every profile we guarantee that the net charge is zero. By applying this procedure, we avoid the uncertainties related to the charge transfer process that is dependent as well on the type, size and concentration of ice particles (Saunders et al., 2006) and focus on the vertical distribution of the charge centers.

2.4 Statistical tests

In order to evaluate the thunderstorm statistical representativeness difference observed between the three chimneys or between the overall profiles against TGF associated thunderstorms we have employed Student´s t-test (Wilks, 2011). In addition, we have computed the Welch variant of the Student´s t-test (Ruxton, 2006) to confirm the representativeness of the statistical test due to the small number of TGF/TRMM matches, Table 1.

In this study, both Student's t-test and Welch variant of the Student´s t-test are used to evaluate the difference of means of two distributions, i.e., the probability that the two means are equal. For this test, the null hypothesis assumes that the two means are equal. The Welch variant of the Student´s t-test uses the same hypothesis but is more robust for unequal variances as well for unequal sample sizes.

As the mean values evaluated could be either higher or lower in respect to another sample, we apply the two-tailed test. The confidence level, statistical significance of the difference of means, is based on the *p-level* (area under the standardized normal distribution) obtained by the Z-score (distance from the mean value in standard deviations of radar reflectivity) and could be expressed as (1-*p-level*)×100%. Z-score is valid for both Student´s t-test and Welch variant and can be expressed as:

$$Z_{score} = \frac{\overline{x_1} - \overline{x_2}}{\sqrt{\frac{\sigma_1^2}{N_1} + \frac{\sigma_2^2}{N_2}}}$$

Where $\bar{x}$ is the mean value of the distribution, σ^2 is the variance of the distribution and N is the number of samples. The subscripts 1 and 2 represent the distributions tested. However, the degrees of freedom (*df*) are different for the two statistical tests and can be expressed as follows:

Student´s t-test

$$df = N_1 + N_2$$

Welch Variant

$$df = \frac{\left[\frac{\sigma_1^2}{N_1} + \frac{\sigma_2^2}{N_2}\right]^2}{\left[\frac{\sigma_1^4}{(N_1 - 1)N_1^2} + \frac{\sigma_2^4}{(N_2 - 1)N_2^2}\right]}$$

For this study, we choose the 95% and 99% confidence levels to state the statistical representativeness of the mean differences for both Student´s t-test and the Welch variant. The p-values and the correspondent confidence levels computed for both Student´s t-test and Welch variant are available in the repository files.

Finally, to evaluate the statistical representativeness of the precipitation profiles and the respective vertical electrical charge structure derived from the TRMM and TGF observation matches in comparison to the Climatological database, we have conducted a Bootstrap analysis that is shown in Appendix D.

3 The structure of the thunderstorms

3.1 Climatology

Table 1 shows that the African continent presents the highest frequency of thunderstorms, followed by America and Southeast Asia, consistent with the climatologies presented by *Boccippio et al.* (2000), *Cecil et al*. (2014) and *Albrecht et al.* (2016). With respect to size and lightning flash rates observed during the TRMM-PR and LIS overpasses, African thunderstorms are smaller (15-20%) but produce much more lightning (1.3-1.9 times more) than the other two areas (see Table 2 and Supplementary Figure S1). It is interesting to note that despite the fact that the differences between the thunderstorm sizes are statistically different, American and Southeast Asian thunderstorms show similar lightning flash rates.

Table 2. Climatological median values [25-75% percentiles in brackets] for thunderstorm radius, number of flashes per thunderstorm and flash density over the 3 regions. LIS flashes correspond to a maximum of 90 seconds of TRMM-LIS view time observation (*Christian et al., 1999*).

Region	Radius (km)	LIS Flashes per thunderstorm	10^3 x LIS Flashes per thunderstorm per km^2
America	29.0 [17.8-52.0]	3 [1-7]	1.2[0.5-3.0]
Africa	22.0 [14.1-38.9]	4 [2-13]	3.0[1.3-6.7]
SE Asia	27.5 [17.6-47.2]	3 [1-7]	1.3[0.5-3.0]

In terms of precipitation vertical structure, the vertical profiles of radar reflectivity factor (Z) in Figure 2a (Figure A1) and the computed echo top height/temperature (Table 3) confirm that African thunderstorms are indeed taller and more vigorous than American and Southeast Asian thunderstorms. For instance, African thunderstorms are up to 1.5-2.8 dBZ more intense between 5 and 15 km height (0 and -72^{o}C), in addition to Z diminishing faster (-2.2 to -1.5 dBZ/km) with altitude than in the other thunderstorms from -15 to -60^{o}C and decrease slower (-2.8 dBZ/km) from 0 to -15^{o}C, Table 4. Moreover, African thunderstorms show as much as 1.2 km higher 30 dBZ echo top height or levels 8-9^{o}C colder than the American and Southeast Asian thunderstorms, Table 3.

The higher Z values and 30 dBZ echo top in addition to the lower dZ/dh values between 0 and -15^{o}C indicate that African thunderstorms present stronger updrafts that produce more super-cooled water droplets and denser ice particles aloft in the entire column, resulting in a deeper and thicker ice layer, thus producing more ice efficiently (*Liu et al*., 2012). In fact, intense vertical velocity helps to produce higher super-saturation, which activates more cloud condensation nuclei and therefore produces more super-cooled water droplets and ice particles (*Korolev*, 2007). Additionally, Z decreases around 1.7 and 3 dBZ/km between 0 and -15 ^{o}C in all three regions, Table 4 and Figure A1, indicating that riming and accretion is active and very effective (*Zipser and Lutz*, 1994; *Yuter and Houze Jr*, 1995; *Heiblum et al*, 2017). Therefore, the charge electrification processes become more efficient (*Takahashi*, 1978; *Saunders et al.*, 2006). Below the freezing level (Figure A1), Z decreases slightly for African thunderstorms, which may imply that evaporation dominates the collision and breakup processes (*Liu and Zipser*, 2013), while in Southeast Asia and America it is balanced. According to *Fabrò et al.* (2019), the African region is drier than the other two areas, consistent with the presented Z profiles.

Table 3. Statistical parameters (mean and confidence level from Student´s t-test) for the 30 dBZ echo top height [temperature] for coincident measurements of TRMM-PR and LIS over the 3 chimneys (Climatology) and for the thunderstorms associated with AGILE, Fermi-GBM and RHESSI TGF detections (TGF Thunderstorms). The statistical test evaluates whether the Climatology and TGF echo top height [temperature]mean differences are significant.

Region	Climatology	TGF Thunderstorms	Confidence Level (%)
America	8.1 km [-19.8^{o}C]	8.7 km [-24.2^{o}C]	88.9 [88.3]
Africa	9.2 km [-27.7^{o}C]	9.1 km [-26.9^{o}C]	12.7 [18.6]
SE Asia	8.0 km [-18.8^{o}C]	8.7 km [-22.4^{o}C]	90.5 [83.3]

In the CFAD panels in Figure 3, it is evident that African (Fig. 3b) thunderstorms present a broader radar reflectivity distribution from surface up to 16 km height in comparison with the other 2 regions. American (Fig. 3a) and SE Asian (Fig. 3c) thunderstorms show narrower Z distributions from 7 to 16 km (-20^{o}C to -60^{o}C, see Figure B1). Using the 5% and 95% percentile to represent the radar reflectivity distribution, it is possible to observe that 30 dBZ is frequent until 14 km height in African and up to 9 km in American and SE Asian thunderstorms. The observed narrower and unimodal (gradient scale with one frequency maximum, see Supplementary Figure S2) radar reflectivity distribution with height (temperature, Figure B1) is characteristic of the mature stage (*Yuter and Houze Jr.*, 1995). The radar reflectivity decay with height above the 0^{o}C isotherm indicates the glaciation process activation and disappearance of the super-cooled water droplets either by freezing or by accretion made by graupel and/or hail particles (*Yuter and Houze Jr.*, 1995)

The CFAD difference plots (Figure 3d and 3f) clearly indicate the vigor of African thunderstorms as these storms have higher reflectivity values with greater frequency of occurrence at all height levels (red scale at Figure 3d and Figure 3f). These features reinforce the fact that African thunderstorms may present a larger variety of size and type of ice crystals, in addition of more super-cooled water droplets between 0^{o}C and -40^{o}C (Figure B1), which helps the electrical charging process, thus producing more lightning. Also, by inspecting the height of 30 dBZ above the freezing level, it is possible to identify the regions in the storm with denser ice particles that are responsible to transfer electrical charges more efficiently (*Takahashi*, 1978; *Saunders et al.*, 2006) and correlate with the production of ice particles and lightning flashes (*Zipser*, 1994; *Petersen et al.*, 1996). Taking into account these features, African thunderstorms clearly show higher frequency of occurrence of 30 dBZ with height, indicating the presence of more and denser ice particles. This particular characteristic can explain the higher lightning activity in comparison with the other 2 chimneys. Moreover, American (Figure 3a) and SE Asian (Figure 3c) thunderstorms show a higher frequency for lower Z values, indicating that they do not form large ice particles, which may explain the lower lightning activity as compared to the African thunderstorms. In addition, the vertical thunderstorm structure observed in these two regions (Figure 3b) is very similar and explains the results shown in Tables 2, 3 and 4, i.e., similar vertical development and lightning activity.

Table 4. Mean [standard deviation] variation of Z with altitude from 0 to -60°C (with 15°C interval) for both Climatology and TGF thunderstorms. The confidence levels represent the statistical significance between the differences of the means of dZ/dh computed for Climatology and TGF thunderstorms using Student´s t-test.

		dZ/dh (dBZ/km)		
Levels		America	Africa	SE Asia
0 to -15°C	Climatology	-2.94 [3.26]	-2.88[3.60]	-3.03[3.36]
	TGF	-2.29[4.62]	-2.25[4.90]	-2.00[4.56]
	Confidence Level (%)	99.98	99.99	100.00
		America	Africa	SE Asia
-15 to -30°C	Climatology	-1.73[3.65]	-2.21[4.04]	-1.77[3.80]
	TGF	-2.47[4.12]	-2.87[4.98]	-2.34[4.38]
	Confidence Level (%)	100.00	99.95	99.96
		America	Africa	SE Asia
-30 to -45°C	Climatology	-1.24[4.37]	-1.52[4.48]	-1.27[4.59]
	TGF	-2.26[4.15]	-2.45[4.84]	-1.91[3.30]
	Confidence Level (%)	100.00	100.00	100.00
		America	Africa	SE Asia
-45 to -60°C	Climatological	-1.35[4.92]	-1.63[4.93]	-1.38[5.02]
	TGF	-2.36[4.32]	-2.29[4.49]	-1.64[4.11]
	Confidence Level (%)	100.00	99.90	83.75

The increased radar reflectivity in the mixed-phase zone (0 and -40°C) and the echo top height/temperature found between the thunderstorms are clearly factors as to why African thunderstorms present higher lightning activity and probably more IC discharges as these features help to produce smaller and less energetic lightning flashes that in principle would not favor TGF as it will be discussed later. These features led African thunderstorms to produce more ice particles and super cooled water droplets aloft that enhances the charge electrification transferring processes. Consequently, opposite polarity charge centers are created at upper levels with short distances of separation. This effect results in more IC discharges with shorter length, thus lower current.

3.2 TGF thunderstorms

As explained in Section 2, the TGF thunderstorm category represents the mean values of the thunderstorms that are close in time and space to the TGF observations. Thus, it has been assumed that it represents the cloud microphysical state of the thunderstorms that produce the TGF. Moreover, as TRMM-TGF thunderstorm matches represent a small sample in comparison to the Climatological database, we have tested its representativeness by computing new Climatological profiles using the bootstrap technique to randomly select the same number of TGF thunderstorms (see

Appendix D for more detailed information) from the Climatological database. This process was conducted for each chimney region, and the statistical test showed a radar reflectivity difference lower than ±0.5-dBZ from 0 to 18 km height. Therefore, the TGF thunderstorm profiles computed are representative of each region.

According to the mean TGF vertical radar reflectivity profiles displayed in Figure 2a (Figure A1), the 3 chimney regions present, analogous shape with Z decreasing around 2.5 – 3 dBZ/km from 4 to 7 km (+2^{o}C to -14^{o}C) and between 0.5-1.5 dBZ/km along the layers of 7 – 14 km (isotherms of -14^{o}C and -67^{o}C). African TGF thunderstorms still have statistically higher reflectivity values than the other two regions (5-12 km for America and 2-14 km for SE-Asia).

In terms of frequency of distributions with altitude, panels a through c of Figure 4 (Figures B2a, B2b and B2c), it is possible to note the similarities between the thunderstorms but also the broader Z distributions observed in the African region from the surface up to 20 km followed by the SE Asia chimney. It is interesting to observe that all three regions present a bimodal distribution (gradient scale with two maximum frequencies of ~13%, see Supplementary Figure S2) above 8-10 km (~ between -20^{o}C and -40^{o}C) with African thunderstorms being shifted towards higher Z values. These signatures aloft indicate that those TGF associated thunderstorms have larger and smaller sized ice particles in the presence of super-cooled water droplets usually related to the developing stages of the storm (*Yuter and Houze* Jr., 1995), favoring the development of a more efficient electrification charging mechanism. This result is consistent with the recent work of *Ursi et al.* (2019) that found larger ice particles in the upper part of TGF thunderstorms and in developing mature phase.

Analyzing the distribution differences between the 3 chimneys, it is clear from the CFAD differences that African thunderstorms have an excessive occurrence of higher Z values above 4 km of altitude (0^{o}C) when comparing with American (Figure 4d) and SE Asian (Figure 4f) regions, especially between 0 and 15 km. SE Asian thunderstorms present a slightly elevated frequency of occurrence for high Z values in contrast to the American region from 5-14 km height (0 and -67^{o}C), Figure 4e (Figure B2e).

3.3 Climatology versus TGF

By comparing the Climatology and TGF thunderstorm vertical profiles between the same regions, Figure 2a, it is found that American TGF thunderstorms have higher reflectivity values, ranging from 0.4-1.1 dBZ from 2 km up to 11.4 km, and SE-Asia TGF thunderstorms show 0.1-1.5 dBZ higher values from 6.4 to 16.4 km height, which are statistically significant. However, the Africa region does not show any statistically significant difference between TGF and Climatology thunderstorms.

In terms of radar reflectivity distribution similarities between the Climatology and TGF thunderstorms, the CFAD differences in Figures 5a, 5b and 5c (Figure B3) indicate that TGF associate thunderstorms have a greater frequency of occurrence of larger Z values from 4 km to 14 km (+2 ^{o}C to -67 ^{o}C). The most pronounced differences are found in the American (Figure 5a) and SE Asian (Figure 5c) continents, especially between 5 and 16 km height. In Africa (Figure 5b), though, the differences are less noticeable although TGFs thunderstorms present a slightly greater occurrence of higher Z values, especially above 12 km (-50^{o}C).

Based on these CFADs (CFTD) differences features, Figure 5 (Figure B3), American and SE Asian Climatology thunderstorms are more skewed to Z values lower than the mean between 0 and -50^{o}C (blue color), while TGF counterparts show higher frequency of occurrence above the mean value within 0 to -70^{o}C (orange color). In Africa though, the highest frequency differences are restricted to -10^{o}C and -80^{o}C, where TGF thunderstorms show slightly higher frequency of occurrence for larger Z values. Moreover, the unimodal and bimodal distributions differences observed in the Climatology and TGF associated thunderstorms are evident. America shows larger differences between -20 and -50^{o}C, African above -40^{o}C and SE Asia limited to -20 and -40^{o}C. These vertical differences reinforce the fact that TGF-associated thunderstorms might present a more efficient charging mechanism displaced upward, and the position of the opposite charging layers may control not only the lightning activity but also the predominant type (intra-cloud or cloud to ground) and consequently the production of TGFs.

In terms of 30 dBZ echo top height and temperature, Table 3, American and SE-Asian TGF thunderstorms are on average 600 m taller and reach as much as 3.5-4.3 ^{o}C cooler levels (with a confidence level above ~90%) when compared to the Climatology storms, while less significant African thunderstorms decrease by 100 meters.

Although the radar reflectivity values with height differ slightly, TGF thunderstorms present similar radar reflectivity decay with height (temperature), regardless of the region (2-2.8 dBZ/km between 0 and -30^{o}C and 1.9-2.4 dBZ/km for -30^{o}C and -60^{o}C) (Table 4), i.e., the difference amongst the 3 regions are not statistical significant. For the Climatology thunderstorms thought, the differences are statistically significant. Lastly, the Z variation with height is statistically different between Climatology and associated TGF in each region, Table 4, except SE Asia below -45^{o}C. These statistical significance tests confirm that associated TGF thunderstorms have specific characteristics and the particular vertical signature (radar reflectivity decay rate) might represent a precipitation feature that distinguishes thunderstorms that produce TGF.

4. Charge structure

Based on the vertical profiles of liquid water content (converted from radar reflectivity factor) and temperature (converted from altitude using Reanalysis-1) we have computed the mean vertical profiles of the normalized electrical charge fraction for the Climatology as well as for the associated TGF thunderstorms upon the non-inductive mechanism proposed by *Takahashi* (1978), which is shown in Figure 6.

The negative and positive charge centers each have a total of 50% of the total charges. The vertical lines at the height plot (a) indicate the altitude levels where the difference of the means (TGF - Climatology) are statistically significant and present a confidence level greater than 95% for each region and for the positive and negative charge layers.

Using the 10-90% percentile cumulative distribution along the estimated vertical electric charge fraction profiles, two main charge centers are distinguished over the observed thunderstorms:

a) Midlevel negative charge center varying from 4.6 to 8.1 km (1.2 to -18.2^{o}C);

b) Upper level positive charge center varying from 7.4 to 14.6 km (-14.2 to -67.5^{o}C).

It is important to note that these two main charge centers are consistent with balloon measurements compiled by *Krehbiel* (1986), *Stolzenburg* et al. (1998) and *MacGorman* et al. (2001) that indicate a middle level negative charge center varying from 0 to -20^{o}C and an upper positive charge center between -15^{o}C up to -40^{o}C.

When comparing the charging fractions between Climatology and TGF associated thunderstorms, the following statistically significant differences are observed in each electrical layer:

- Positive charge layer: America shows a statistically significant difference between 6-7 km, 7-10 km, 11-14 km and 15-16 km, Africa from 6-10 km and 11-17 km, and SE-Asia from 6-8 km, 9-14 km and 15-16 km.

- Negative charge layer – America presents statistically significant differences between 5-7 km and 8-10 km, Africa from 4-5 km, 6-8 km and from 9-10 km, and SE-Asia from 4-7 km.

TGF thunderstorms show a vertical upward displacement of the positive charge center (median charge height layer as a reference) by 300 to 500 m (1.6 to 4.0 ^{o}C colder). As a result, the distance between the negative and positive charge centers varies from 4.4-4.5 km for Climatology thunderstorms to 4.7-4.9 km for TGF-associated thunderstorms, reinforcing the fact that thunderstorms that produce TGF are expected to show more vertically separated charging centers, which are associated with higher altitude electrical charge regions (*Fabró et al.,* 2019), thus more energetic lightning flashes (*Cummer et al*., 2015). Additionally, TGF thunderstorms show slightly thicker (300-700 m) positive charge layers when comparing against Climatology thunderstorms.

Analyzing the vertical distribution of the charge fraction with temperature, Figure 6b, the African thunderstorms do show more positive cumulative charge fraction from 0 to -40^{o}C and less at temperatures below -40^{o}C. This difference can reach as much as 5-9% between 0 and -20^{o}C where the cumulative negative charge fraction is above 96%. Therefore, African thunderstorms have higher probability to produce shorter and more frequent IC lightning flashes as the opposite charge centers are closer. Therefore, longer and vertically oriented IC flashes will be less frequent due to lower positive charges above -40^{o}C. This particular feature could explain the higher IC flash rates observed in African thunderstorms and the lower TGF efficiency as proposed by *Fabró et al.* (2019).

Using the radar reflectivity profile as a function of temperature (Figure A1) and the CFTD differences (Figure B3), it can be speculated that the decrease in the charge density between -20 ^{o}C and -40^{o}C inferred in the TGF thunderstorms (Figure 6b) is caused by a reduction in graupel/hail production (Z decays slightly more with height), which reduces the size or concentration of these dense ice particles (Figure B3 - TGF thunderstorms show a higher frequency of occurrence of Z values under the mean Climatology values). On the other hand, the charge fraction enhancement at temperatures below -40^{o}C might be an effect of the smaller ice particles transported upward that collided with smaller graupel/hail particles formed in the mixed zone and retained the positive charges while graupel and hail became negatively charged.

4 TGF Paradox Discussion

To shed some light on the TGF paradox this study proposed to answer two questions which are now addressed:

a) Does the vertical distance between the electrical charge centers dictate the production of TGF?

In comparison to the climatological database, TGF related thunderstorms show higher 30 dBZ echo heights, Z profiles are as much as 0.5-1.5 dBZ higher, have a greater frequency of occurrence of higher radar reflectivity values with height, show the presence of both ice and super-cooled water droplets above 8 km height (bimodal distribution), and finally a larger Z gradient (dZ/dh is higher), meaning that they are more efficient ice producers. These features are in general associated with storms growing in a developing to mature stage where stronger updrafts are present. These dynamic mechanisms lead to an enhanced electrification charging transfer associated with vertical expansion and upward displacement of the electrical charging layers. In fact when analyzing the inferred vertical electrical structure, TGF thunderstorms presented 300-700 meters thicker positive charge layers and greater vertical distances (up to 500 meters) between two opposite charge centers. By having more charges in the electrical charging layer that became more apart, the electrical field builds up and may help the development of more energetic vertical IC lighting discharges.

b) Does the vertical structure of thunderstorms explain the TGF to lightning flash rate asymmetry observed in the 3 chimneys?

In terms of regional differences, the precipitation vertical profiles of radar reflectivity clearly indicate that African thunderstorms are taller (30 dBZ height) and more intense (1.5-2.8 dBZ). Additionally, in these thunderstorms Z falls slower with height (-2.8 dBZ/km) from 0 to -15^{o}C and faster (-2.2 to -1.5 dBZ) from -15 to -60^{o}C. Moreover, African thunderstorms are smaller (up to 20%) and can produce as 80% more lightning discharges than the other two regions. The CFAD and CFTDs diagrams revealed that American and SE Asian thunderstorms have more ice between 0 and -50^{o}C while African thunderstorms are distributed between the isotherms of -20 and -80 ^{o}C. Moreover, these diagrams showed a bimodal distribution bounded by the -20 and -40 ^{o}C isotherms, with African thunderstorms being broader and more intense. These features indicate the presence of super cooled water droplets and ice particles that are more abundant in African thunderstorms. As a result, African thunderstorms have a more efficient electrification mechanism that helps to produce more lightning discharges than American and Southeast Asian thunderstorms. Furthermore, as African thunderstorms have more super-cooled water droplets between 0 and -15^{o}C due to higher Z values and lower absolute dZ/dh, the charge transfer would more efficient. Thus, it helps to produce more lightning flashes in the lower part of the cloud, which represents in smaller ICs flashes and CG discharges.

In terms of the electrical charge fraction, it was found that African TGF thunderstorms presented more cumulative positive charge fraction between 0 to -20^{o}C and lower at temperatures below -40^{o}C. As result, the lower part of the positive layer that has more charges is closer to the negative layer, thus allowing to reach the electric field necessary to dielectric breakdown with lower amounts of charge. As a consequence, this arrangement permits African TGF thunderstorms to produce more and shorter IC lightning flashes with less current in the lower part of the cloud. In another hand, less frequent due to lower cumulative charge fraction, the upper portion of the positive charge layer is more distant thus helping to produce larger and consequently more energetic IC lightning flashes as well increasing the large-scale electric fields in the storm, which could be associated with the development of TGF. As result, this type of charge disposition may explain why African thunderstorms produce fewer TGFs per lightning flashes than the other two regions.

5 Concluding Remarks

We presented a statistical study that analyzed the vertical structure of thunderstorms observed in 9,772 TRMM PR orbits to elucidate the TGF versus lightning occurrence asymmetry observed between the 3 major tropical thunderstorm regions. Mean profiles were computed using TRMM PR and LIS coincident measurements from 1998 to 2014. TGFs detected by AGILE, Fermi-GBM and RHESSI instruments were used as proxies to select the most probable associated precipitation feature in the field of view of these sensors.

According to the vertical precipitation structures in convection over the America, Africa and Southeast Asia regions, African thunderstorms present a higher concentration of precipitating sized super-cooled water droplets and ice particles above the freezing level as these thunderstorms show higher Z values (1.5-2.8 dBZ) above the 0^{o}C isotherm. The CFAD diagrams showed unimodal and narrow radar reflectivity distributions with height indicating a mature stage of convection (*Yuter and Houze Jr*, 1995). African thunderstorms are smaller (5-20%), 1.2 km taller, and 9 ^{o}C colder (30 dBZ echo top height). Furthermore, taking into account LIS measurements, African thunderstorms produce almost 30-80% more lightning flashes than their American and Southeast Asian counterparts. These results are consistent previous finding that showed that African thunderstorms present higher frequency of occurrence of overshooting deep convection due to larger volume and ice mass (*Liu and Zipser*, 2005) and higher number of lightning flash rates per second per convective cloud for the same freezing cloud depth (*Yoshida et al.*, 2009).

TGF-related thunderstorms present similar radar reflectivity decay with height and temperature independently of the region (2-2.8 dBZ/km in the layer of 0 and -30^{o}C and 1.9-2.4 dBZ/km in the layer of -30^{o}C and -60^{o}C). The radar reflectivity distributions with height pointed to the presence of a bimodal distribution above -20^{o}C, probably the presence of ice particles and super-cooled water droplets, a characteristic of thunderstorms in developing stages (*Yuter and Houze Jr*, 1995).

In general, TGF thunderstorms are more intense (by 0.5-1.5 dBZ) and taller (30 dBZ echo height) with respect to the Climatology. Within the TGF thunderstorm profiles, Africa tends to resemble the other two regions in vertical shape despite being more intense in terms of radar reflectivity (1-2 dBZ). Moreover, it should be mentioned that Climatology includes all the convective stages of thunderstorms, and the fact that we find stronger/taller and bimodal radar reflectivity distributions is above all a sign that the thunderstorms with TGF in view were probably closer to developing to full maturity stages.

After estimating the electric charge layer altitudes by employing *Takahashi's* (1978) scheme, it is possible to state that the microphysical mechanisms of clouds contribute to the production of TGFs. Basically, the partitioning of water and ice in the mixed region changes the height and distance between the positive and negative charge centers. In fact, TGF thunderstorms have thicker charge layers separated by a distance of 4.7-4.9 km while the Climatology set of storms has a distance of 4.4-4.5 km. Additionally, TGF thunderstorms presented up to 700 meter vertical expansion in the positive charge layer. In terms of temperature, the positive charge fraction decreases between -20^{o}C and -40^{o}C and increases at levels above -40^{o}C in the associated TGF thunderstorms. This result may be related to the low production in the mixed region of graupel and hail particles that collide with small ice particles formed either by water vapor deposition or by aggregation and are carried out to the upper levels of the storm.

These features are consistent with the findings of *Barnes et al.* (2015), who showed that TGF-related thunderstorms have higher precipitating ice and cloud ice concentrations above 9 km in comparison with non-TGF thunderstorms. More recently, *Ursi et al.* (2019) also found larger size ice particles in the upper region of TGF thunderstorms, which were associated with their development to a mature stage.

Lastly, African TGF thunderstorms present different positive charge configuration than the other two tropical chimneys that may explain why they produce less TGFs per lightning flash rate. Basically, African TGF thunderstorms show more cumulative positive charge fraction at temperatures warmer than -20^{o}C and lower at levels colder than -40^{o}C. As result, more frequent IC lightning discharges are produced in the lower part, which will carry less current due to short length. In another hand, less frequent, longer IC lightning flashes are produced between the negative charge layer and the upper part of the positive layer. In general, this configuration supports the presence of larger regions with high electric fields in the thundercloud allowing longer vertical propagation of IC flashes (e.g. *Krehbiel et al.* 2008, *Fabró et al.,* 2019) and producing low flash rates (*Bruning and MacGorman* 2013). These features can favour the occurrence of TGF due to the development of more energetic intracloud discharges with longer path to breakdown involving lightning leaders with high electric potentials (e.g. Williams et al. 2006, Celestin and Pasko 2011, *Cummer et al*., 2015; *Smith et al*., 2018 and recently by *Köhn et al.* 2020) and the influence due to the enhancement of the large-scale thunderstorm electric fields on electron acceleration in runaway electron avalanche multiplication theories (e.g. *Dwyer et al.,* 2012). Our results might also justify the longer inter-flash time interval observed prior to TGF (*Larkey et al.*, 2019).

Acknowledgements

This work was supported by the following research grants: Brazilian Research Agencies - Conselho Nacional de Desenvolvimento Científico e Tecnológico (CNPq) [grant numbers: 310489/2006-7] and Coordenação de Aperfeiçoamento de Pessoal de Nível Superior (CAPES) – Programs PROEX and PrInt (grant number: 88887.370081/2019-00); Spanish Ministry of Economy and the European Regional Development Fund (FEDER): ESP2013-48032-C5-3-R, ESP2015-69909-C5-5-R, ESP2017-86263-C4-2-R and PID2019-109269RB-C42. The authors are grateful to TRMM Science Data and Information System (TSDIS) of Goddard Space Flight Center for providing TRMM/PR orbits, to the Lightning and Atmospheric Electricity Group at NASA's Marshall Space Flight Center for their support of the TRMM/LIS data files, to National Centers for Environmental Information (NOAA) for providing NCEP/NCAR Reanalysis (Reanalysis-1), to the Italian Space Agency for providing AGILE TGF data, to David Smith at the University of California, Santa Cruz, for making available RHESSI TGF collection and to NASA Fermi-GBM´s Mission for Fermi-GBM TGF database. The mean profiles (radar reflectivity and electrical charge fraction) and respective statistical tests retrieved in this manuscript are publicly available on the STORM-T Laboratory website data repository at https://www.storm-t.iag.usp.br/pub/TGF-Paradox.

References

Albrecht, R. I., Goodman, S. J., Buechler, D. E., Blakeslee, R. J., & Christian, H. J. (2016). Where are the lightning hotspots on Earth?. *Bulletin of the American Meteorological Society*, *97*(11), 2051-2068.

Awaka, J., T. Iguchi, H. Kumagai, and K. Okamoto (1997). Rain type classification algorithm for TRMM precipitation radar. *Proc. 1997 Int. Geoscience and Remote Sensing Symp.,* Singapore, IEEE, 1633–1635.

Barnes, DE, Splitt, ME, Dwyer, JR, Lazarus, S, Smith, DM, and Rassoul, HK (2015), A study of thunderstorm microphysical properties and lightning flash counts associated with terrestrial gamma-ray flashes. *J. Geophys. Res. Atmos.*, 120, 3453– 3464. doi: 10.1002/2014JD021495.

Battan, L. J. (1973). *Radar observation of the atmosphere* (No. 04; QC973. 5, B3.).

Boccippio, D. J., Goodman, S. J., & Heckman, S. (2000). Regional differences in tropical lightning distributions. *Journal of Applied Meteorology*, *39*(12), 2231-2248.

Briggs, M.S., Fishman, G.J., Connaughton, V., Bhat, P.N., Paciesas, W.S., Preece, R.D., Wilson-Hodge, C., Chaplin, V.L., Kippen, R.M., Von Kienlin, A. and Meegan, C.A. (2010). First results on terrestrial gamma ray flashes from the Fermi Gamma-ray Burst Monitor. *Journal of Geophysical Research: Space Physics*, *115*(A7).

Bruning, E. C., & MacGorman, D. R. (2013). Theory and observations of controls on lightning flash size spectra. *Journal of the Atmospheric Sciences*, *70*(12), 4012-4029.

Cecil, D. J., Buechler, D. E., & Blakeslee, R. J. (2014). Gridded lightning climatology from TRMM-LIS and OTD: Dataset description. *Atmospheric Research*, *135*, 404-414.

Celestin, S., and Pasko, V.P. (2011): Energy and fluxes of thermal runaway electrons produced by exponential growth of streamers during the stepping of lightning leaders and in transient luminous events. Journal of Geophysical Research: Space Physics 116.

Christian, H., Blakeslee, R., Goodman, S., Mach, D., Stewart, M., Buechler, D., Koshak, W., Hall, J., Boeck, W., Driscoll, K. and Bocippio, D.J. (1999 June). The lightning imaging sensor. In *NASA conference publication* (pp. 746-749). NASA..

Cummer, S. A., Zhai, Y., Hu, W., Smith, D. M., Lopez, L. I., & Stanley, M. A. (2005). Measurements and implications of the relationship between lightning and terrestrial gamma ray flashes. *Geophysical Research Letters*, 32, L08811. https://doi.org/10.1029/2005GL022778.

Cummer, S.A., Lyu, F., Briggs, M.S., Fitzpatrick, G., Roberts, O.J. and Dwyer, J.R. (2015). Lightning leader altitude progression in terrestrial gamma-ray flashes. *Geophysical Research Letters*, *42*(18), pp.7792-7798.

Dwyer, Joseph & Smith, David & Cummer, Steven. (2012). High-Energy Atmospheric Physics: Terrestrial Gamma-Ray Flashes and Related Phenomena. Space Science Reviews. 173. 10.1007/s11214-012-9894-0.

Fabró Tàpia, F., Montañá Puig, J., der Velde, V., Arnoud, O., Pineda Rüegg, N., & Williams, E. R. (2019). On the TGF/lightning ratio asymmetry. *Journal of geophysical research: atmospheres*, 1-31.

Fishman, G. J., Bhat, P. N., Mallozzi, R., Horack, J. M., Koshut, T., Kouveliotou, C., ... & Goodman, S. J. (1994). Discovery of intense gamma-ray flashes of atmospheric origin. *Science*, *264*(5163), 1313-1316.

Fuschino, F., Marisaldi, M., Labanti, C., Barbiellini, G., Del Monte, E., Bulgarelli, A., Trifoglio, M., Gianotti, F., Galli, M., Argan, A. and Trois, A. (2011). High spatial resolution correlation of AGILE TGFs and global lightning activity above the equatorial belt. *Geophysical research letters*, *38*(14)..

Gjesteland, T., N. Østgaard, a. B. Collier, B. E. Carlson, C. Eyles, and D. M. Smith (2012), A new method reveals more TGFs in the RHESSI data, Geophysical Research Letters, 39 (5), doi:10.1029/2012GL050899.

Heiblum, R. H., Koren, I., Altaratz, O., & Kostinski, A. B. (2017). The consistent behavior of tropical rain: Average reflectivity vertical profiles determined by rain top height. *Journal of Hydrometeorology*, *18*(3), 591–609.

Iguchi T, Kozu T., Meneghini R., Awaka J., Okamoto K.I. (2000). Rain-profiling algorithm for the TRMM precipitation radar. *Journal of Applied Meteorology*. 39(12):2038-52.

Kalnay, E., Kanamitsu, M., Kistler, R., Collins, W., Deaven, D., Gandin, L., Iredell, M., Saha, S., White, G., Woollen, J. and Zhu, Y. (1996). The NCEP/NCAR 40-year reanalysis project. *Bulletin of the American meteorological Society*, *77*(3), pp.437-472.

Korolev, A. (2007). Limitations of the Wegener–Bergeron–Findeisen mechanism in the evolution of mixed-phase clouds. *Journal of the Atmospheric Sciences*, *64*(9), 3372-3375.

Krehbiel, Paul R., "The Electrical Structure of Thunderstorms," Ch. 8 in The Earth's Electrical Environment, National Academy Press, Washington, 1986.

Krehbiel, P. R., Riousset, J. A., Pasko, V. P., Thomas, R. J., Rison, W., Stanley, M. A., Edens, H. E. (2008): Upward electrical discharges from thunderstorms, *Nature Geoscience,* **1,** 233.

Köhn, C., Heumesser, M., Chanrion, O., Nishikawa, K. ,Reglero, V., Neubert, T. (2020). The Emission of Terrestrial Gamma Ray Flashes From Encountering Streamer Coronae Associated to the Breakdown of Lightning Leaders. Geophysical Research Letters. 47. 10.1029/2020GL089749

Kummerow, C., Barnes, W., Kozu, T., Shiue, J., & Simpson, J. (1998).The tropical rainfall measuring mission (TRMM) sensor package. *Journal of atmospheric and oceanic technology*, *15*(3), 809-817.

Larkey, R. K., Sample, J. G.,Smith, D. M., Briggs, M. S.,Lapierre, J. L., & Holzworth, R. H.(2019). Evidence for extended charging periods prior to terrestrial gamma ray flashes. *Geophysical Research Letters*, *46* https://doi.org/10.1029/2019GL083827.

Liu, C., & Zipser, E. J. (2005). Global distribution of convection penetrating the tropical tropopause. *Journal of Geophysical Research: Atmospheres*, *110*(D23).

Liu, C., & Zipser, E. J. (2013). Why does radar reflectivity tend to increase downward toward the ocean surface, but decrease downward toward the land surface? *Journal of Geophysical Research: Atmospheres*, *118*, 135–148. https://doi.org/10.1029/2012JD018134

Liu, C., Cecil, D. J., Zipser, E. J., Kronfeld, K., and Robertson, R. (2012), Relationships between lightning flash rates and radar reflectivity vertical structures in thunderstorms over the tropics and subtropics, *J. Geophys. Res.*, 117, D06212, doi:10.1029/2011JD017123.

MacGorman, D. R., Straka, J. M., & Ziegler, C. L. (2001). A Lightning Parameterization for Numerical Cloud Models, *Journal of Applied Meteorology*, *40*(3), 459-478.

Marisaldi, M., Fuschino, F., Labanti, C., Galli, M., Longo, F., Del Monte, E., Barbiellini, G., Tavani, M., Giuliani, A., Moretti, E. and Vercellone, S. (2010). Detection of terrestrial gamma ray flashes up to 40 MeV by the AGILE satellite. *Journal of Geophysical Research: Space Physics*, *115*(A3)..

Marisaldi, M., Galli,M., Labanti, C., Ostgaard, N., Sarria, D., Cummer, S. A., et al. (2019). On the high-energy spectral component and fine time structure of terrestrial gamma-ray flashes. *Journal of Geophysical Research: Atmospheres*, 124, 7484–7497. https://doi.org/10.1029/2019JD030554

Masunaga, H., Iguchi, T., Oki, R., & Kachi, M. (2002). Comparison of rainfall products derived from TRMM microwave imager and precipitation radar. *Journal of applied meteorology*, *41*(8), 849-862.

Morales Rodriguez, C. A. (2019). Thunderstorm efficiency regimes in South America as observed by STARNET and TRMM. *Journal of Geophysical Research: Atmospheres*, 124, 11428– 11451. https://doi.org/10.1029/2019JD030950

Østgaard, N., Neubert, T., Reglero,V., Ullaland, K., Yang, S., Genov, G.,et al. (2019). First 10 months of TGF observations by ASIM. *Journal of Geophysical Research: Atmospheres*,124. https://doi.org/10.1029/2019JD031214.

Petersen, W. A., Rutledge, S. A., & Orville, R. E. (1996). Cloud-to-Ground Lightning Observations from TOGA COARE: Selected Results and Lightning Location Algorithms, *Monthly Weather Review*, *124*(4), 602-620.

Philander, S. G. (1989). El Niño, La Niña, and the southern oscillation. *International geophysics series*, *46*, X-289.

Rosenfeld, D., & Ulbrich, C. W. (2003). Cloud microphysical properties, processes, and rainfall estimation opportunities. *Meteorological Monographs*, *52*, 237–258.

Ruxton, G.D. (2006). The unequal variance *t*-test is an underused alternative to Student's *t*-test and the Mann–Whitney *U* test, *Behavioral Ecology*, Volume 17, Issue 4, July/August 2006, Pages 688–690, https://doi.org/10.1093/beheco/ark016.

Saunders, C. P. R., Bax-Norman, H., Emersic, C., Avila, E. E., & Castellano, N. E. (2006). Laboratory studies of the effect of cloud conditions on graupel/crystal charge transfer in thunderstorm electrification. *Quarterly Journal of the Royal Meteorological Society: A journal of the atmospheric sciences, applied meteorology and physical oceanography*, *132*(621), 2653-2673.

Smith, D. M., Bowers, G. S., Kamogawa, M., Wang, D., Ushio, T., Ortberg, J., ... & Stock, M. (2018). Characterizing upward lightning with and without a terrestrial gamma ray flash. *Journal of Geophysical Research: Atmospheres*, *123*(20), 11-321.

Smith, D.M., Lopez, L.I., Lin, R.P. and Barrington-Leigh, C.P. (2005). Terrestrial gamma-ray flashes observed up to 20 MeV. *Science*, *307*(5712), pp.1085-1088.

Splitt ME, Lazarus SM, Barnes D, Dwyer JR, Rassoul HK, Smith DM, Hazelton B, Grefenstette B. (2010), Thunderstorm characteristics associated with RHESSI identified terrestrial gamma ray flashes. *Journal of Geophysical Research: Space Physics*. 2010 Jun 1;115(A6).

Stolzenburg, M., Rust, W. D., and Marshall, T. C. (1998), Electrical structure in thunderstorm convective regions: 2. Isolated storms, *J. Geophys. Res.*, 103(D12), 14079– 14096, doi:10.1029/97JD03547.

Takahashi, T. (1978). Riming electrification as a charge generation mechanism in thunderstorms. *Journal of the Atmospheric Sciences*, *35*(8), 1536-1548.

Ursi, A., Marisaldi, M., Dietrich, S., Tavani, M., Tiberia, A., & Porcu, F. (2019). Analysis of Thunderstorms Producing Terrestrial Gamma Ray Flashes With the Meteosat Second Generation. *Journal of Geophysical Research: Atmospheres*, *124*(23), 12667-12682.

Wilks, D. S. (2011). *Statistical methods in the atmospheric sciences*, (2nd ed.p. 627). Boston: Elsevier, Academic Press.

Williams, E., Boldi, R., Bór, J., Sátori, G., Price, C., Greenberg, E., Takahashi, Y., Yamamoto, K., Matsudo, Y., Hobara, Y., et al. (2006): Lightning flashes conducive to the production and escape of gamma radiation to space. Journal of Geophysical Research Atmospheres 111.

Yoshida, S., Morimoto, T., Ushio, T., & Kawasaki, Z. (2009). A fifth-power relationship for lightning activity from Tropical Rainfall Measuring Mission satellite observations. *Journal of Geophysical Research: Atmospheres*, *114*(D9).

Yuter, S. E., & Houze Jr, R. A. (1995). Three-dimensional kinematic and microphysical evolution of Florida cumulonimbus. Part II: Frequency distributions of vertical velocity, reflectivity, and differential reflectivity. *Monthly weather review*, *123*(7), 1941-1963.

Zipser, E. J. (1994). Deep Cumulonimbus Cloud Systems in the Tropics with and without Lightning, *Monthly Weather Review*, *122*(8), 1837-1851.

Zipser, E. J., & Lutz, K. R. (1994). The Vertical Profile of Radar Reflectivity of Convective Cells: A Strong Indicator of Storm Intensity and Lightning Probability?, *Monthly Weather Review*, *122*(8), 1751-1759.

Appendix A – Vertical profiles as a function of temperature

Figure A1. Mean vertical radar reflectivity (left) and respective standard deviations (right) profiles for convective rain type as a function of temperature in the 3 chimneys: America (blue), Africa (red) and Southeast Asia (orange). Climatology profiles are continuous line and associated thunderstorms with TGF detections are in dashed lines.

Appendix B – Contoured Frequency by Temperature Diagrams – CFTD

Figure B1. CFTD depicted for the thunderstorms observed in America (a), Africa (b) and Southeast Asia (c) region characterized as Climatology. CTFD differences between the three regions: (d) America - Africa, (e) America - SE Asia and (f) SE Asia - Africa.

Figure B2. CFTD depicted for the associated TGF thunderstorms observed in America (a), Africa (b) and Southeast Asia (c) region characterized as Climatology. CFTD differences between the three regions: (d) America - Africa, (e) America - SE Asia and (f) SE Asia – Africa.

Figure B3. CFTD differences between Climatology and associated TGF thunderstorms for each tropical chimney: (a) America, (b) Africa and (c) SE Asia.

Appendix C: TGFs observed by AGILE, FERMI-GBM and RHESSI

For statistical reference on the complexity of finding TGF matches on TRMM observations, Table C1 presents the total number of TGFs detected by the 3 satellite missions over the globe as well as over the 3 chimney regions during the 2002-2014 period. Moreover, Table C1 shows the total number of TRMM orbits during TGF observations and those that had active thunderstorms. Although there are more than five thousand observed TGFs in the world by the 3 missions (Figure 1), only 32% of the TGFs were observed in the 3 chimney regions, and just 16% of those 1749 TGFs had TRMM-PR coincident matches under the defined criteria. Finally, of these 286 (16%) TRMM PR and LIS orbits, only 124 (43%) had active thunderstorms (with LIS lightning flashes) within 600 km from AGILE, Fermi-GBM or RHESSI satellite footprint position.

Table C1. Number of TGFs observed by AGILE, Fermi-GBM and RHESSI over the globe during the period of 2002 to 2014, followed by the number of TGFs over the 3 chimney regions, with matched TRMM orbits and matched TRMM orbits with LIS lightning observations.

TGF Missions	Observed TGFs over the globe	TGFs observed in the 3 chimney regions	TRMM matched orbits with TGFs in the 3 chimney regions	TRMM matched orbits with TGFs in the 3 chimney regions with storms with LIS lightning flashes observation within 600 km
Fermi-GBM (2008-2014)	4136	1232	82	25
AGILE (2009-2012)	308	189	53	42
RHESSI (2002-2010)	976	328	151	57

Appendix D – Bootstrap analysis

A bootstrap analysis (Wilks, 2011) was employed to evaluate whether the precipitation structure and the corresponding electrical charge fraction computed for the TGF thunderstorms can represent the mean state of the thunderstorms that were active during the observation of a TGF when compared to the Climatology profiles.

Bootstrap analysis consists of performing random selections of N samples several times to compute a mean value. By applying this procedure, it is possible to evaluate whether the mean value of a data set with N samples has statistical representativeness and it is statistically different from a Climatological database.

For this study, the bootstrap analysis was configured to randomly select thunderstorms for each region and to compute a mean profile based on the Climatological database built (Table 1). This process was repeated 100 times to finally obtain the mean bootstrap profile. For each of the 100 simulations, we randomly selected 35 thunderstorms in the American region, 43 in Africa, and 46 in Southeast Asia (i.e. the same number of TGF cases) from the Climatological database and computed a mean profile for each chimney. The new mean regional profile was then denoted as bootstrap profile. This procedure was made to compute both the mean radar reflectivity profile and the respective electrical charge fraction.

As a first step, we compared the mean Climatological radar reflectivity profile for each region with the corresponding bootstrap profile that was computed with the same number of samples of TRMM/TGF matches. Therefore, if the radar reflectivity profiles are different it means that the mean profile computed with the same number of TGF samples does not have statistical representativeness; otherwise, it does show statistical significance.

To analyze such statistical representativeness, Figure D1 shows a comparison between the Climatological and the bootstrap profiles for the thunderstorms in America, Africa and Southeast Asia, i.e., the difference among the two profiles (Climatological and bootstrap). According to these plots, the radar reflectivity differences are lower than ± 0.5 dBZ in the SE-Asian thunderstorms and from 0 to 18 km to American and African thunderstorms. The values between ± 0.5 and 1 dBZ at 18-20 km might be attributed to the low samples at these altitude levels. Therefore the Climatological profiles are representative, and the N TRMM/TGF match samples is sufficient to characterize the region.

Figure D1. Difference between the Climatological and Bootstrap mean vertical convective radar reflectivity profile computed for the 3 chimneys: America, Africa and Southeast Asia.

As a second and final evaluation, we compared the differences between the Climatology and bootstrap profiles in terms of the electrical charge fraction, Figure D2. To facilitate the analysis we separately present positive and negative charge fraction differences. According to these results, there are no significant differences between the Climatology and bootstrap profiles, i.e., the positive charge fraction is within ± 0.2% while the negative charge fraction is mainly between ± 0.1%. These results lead us to conclude that the Climatology and TGF profiles can be used to illustrate the mean feature of thunderstorms observed in Africa, America and SE-Asia.

Figure D2. Difference between the Climatology and bootstrap charge fraction profiles for each chimney (America – blue; Africa – red; and SE Asia – orange). The left panel shows the difference between the positive charge fraction and the right panel the negative charge fraction.

These results reinforce the fact that the observed differences on radar reflectivity and electrical charge fraction between the TGF associated thunderstorms and Climatology are statically representative.

Figure 1. Number of TGFs detected on 1 x 1 grid box by the AGILE, Fermi-GBM and RHESSI missions during the 2002-2014 period. The 3 boxes sketched correspond to the 3 tropical lightning chimneys with maximum TGF activity as observed by *Fabró et al.* (2019).

Figure 2. (a) Mean vertical radar reflectivity and (b) respective standard deviations (right) profiles for convective rain type as a function of height in the 3 chimneys: America (blue), Africa (red) and Southeast Asia (orange). Climatology profiles are the continuous lines and thunderstorms associated with TGF detections are in dashed lines.

Figure 3. (Top) Climatological radar reflectivity factor CFADS for America (a), Africa (b) and SE Asia (c) thunderstorm regions. The lines in the CDADs indicate the percentiles of 5, 50 e 95%. (Bottom) CFAD difference plots show a comparison between the 3 chimneys: (d) America versus Africa, (e) America versus SE Asia and (f) SE Asia versus Africa. The respective mean radar reflectivity profiles for each region are shown on the CFAD difference plots (America – continuous line, Africa – dashed line, SE Asia - dashed with dots and diamond symbol line).

Figure 4. Same as Figure 3 but for thunderstorms associated with the TGF occurrence.

Figure 5. CFAD differences between Climatology and associated TGF thunderstorms for each tropical chimney.

Figure 6. Mean vertical profile of charge fraction estimated for all 3 chimneys (Climatology - continuous lines) and TGF triggered thunderstorms (dashed lines) based on *Takahashi* (1978) scheme as a function of height (a) and temperature (b).

Figure A1. Mean vertical radar reflectivity (left) and respective standard deviations (right) profiles for convective rain type as a function of temperature in the 3 chimneys: America (blue), Africa (red) and Southeast Asia (orange). Climatology profiles are continuous line and associated thunderstorms with TGF detections are in dashed lines.

Figure B1. CFTD depicted for the thunderstorms observed in America (a), Africa (b) and Southeast Asia (c) region characterized as Climatology. CTFD differences between the three regions: (d) America - Africa, (e) America - SE Asia and (f) SE Asia - Africa.

Figure B2. CFTD depicted for the associated TGF thunderstorms observed in America (a), Africa (b) and Southeast Asia (c) region characterized as Climatology. CFTD differences between the three regions: (d) America - Africa, (e) America - SE Asia and (f) SE Asia – Africa.

Figure B3. CFTD differences between Climatology and associated TGF thunderstorms for each tropical chimney: (a) America, (b) Africa and (c) SE Asia.

Figure D1. Difference between the Climatological and Bootstrap mean vertical convective radar reflectivity profile computed for the 3 chimneys: America, Africa and Southeast Asia.

Figure D2. Difference between the Climatology and bootstrap charge fraction profiles for each chimney (America – blue; Africa – red; and SE Asia – orange). The left panel shows the difference between the positive charge fraction and the right panel the negative charge fraction.

Figure 1.

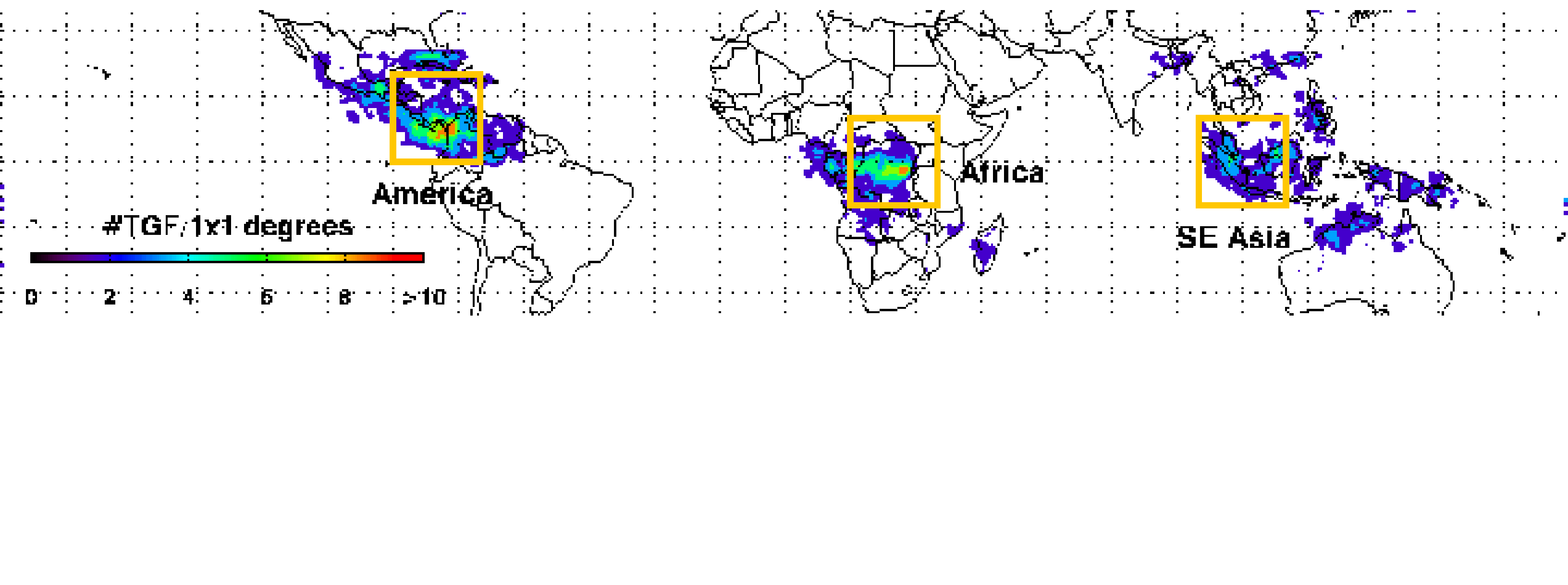
America
Africa
SE Asia
#TGF/1x1 degrees
0
2
4
6
8
>10

Figure 2.

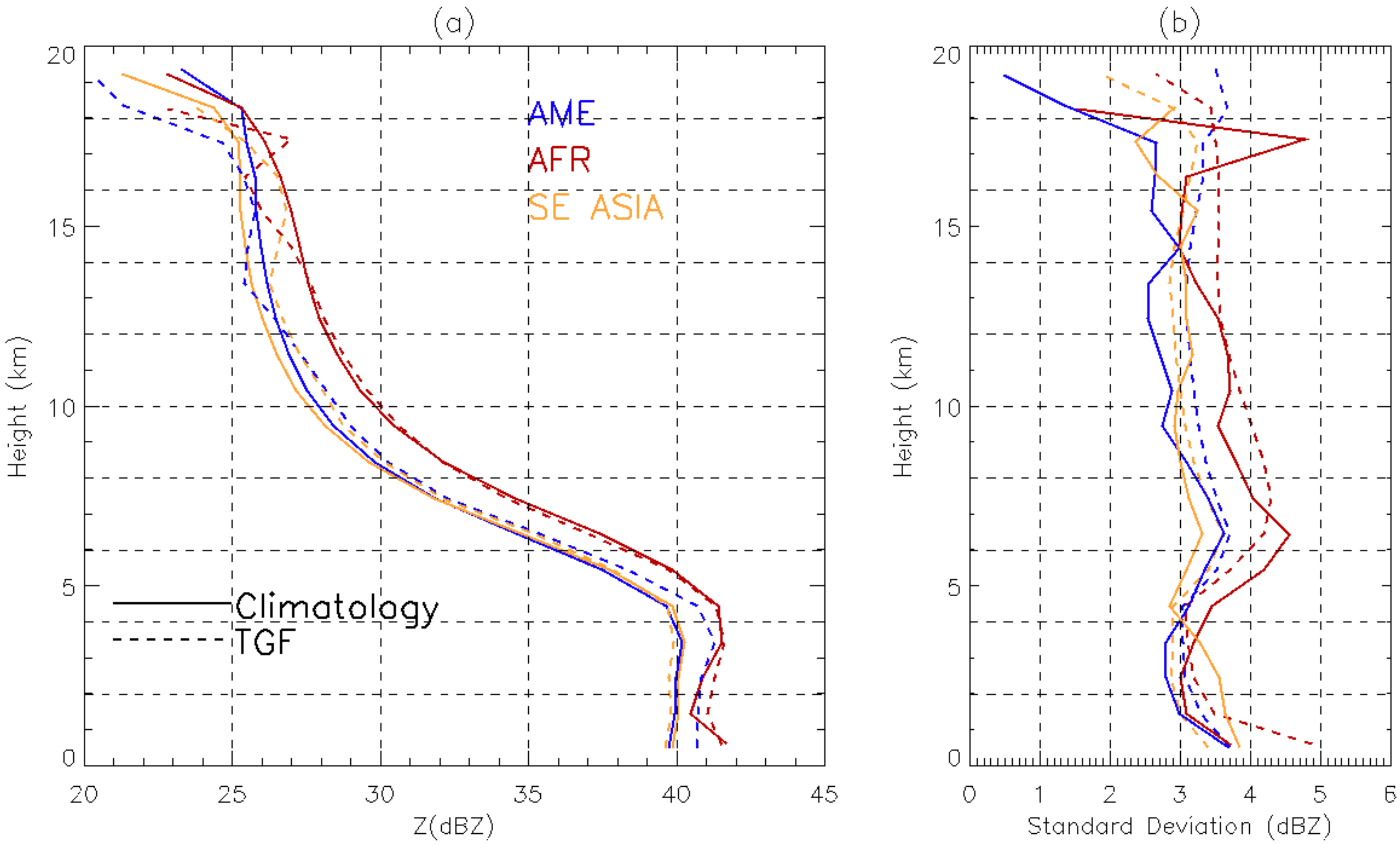

(a)
(b)
AME
AFR
SE ASIA
Climatology
TGF
Height (km)
Z(dBZ)
Standard Deviation (dBZ)
0
5
10
15
20
25
30
35
40
45
1
2
3
4
6

Figure 3.

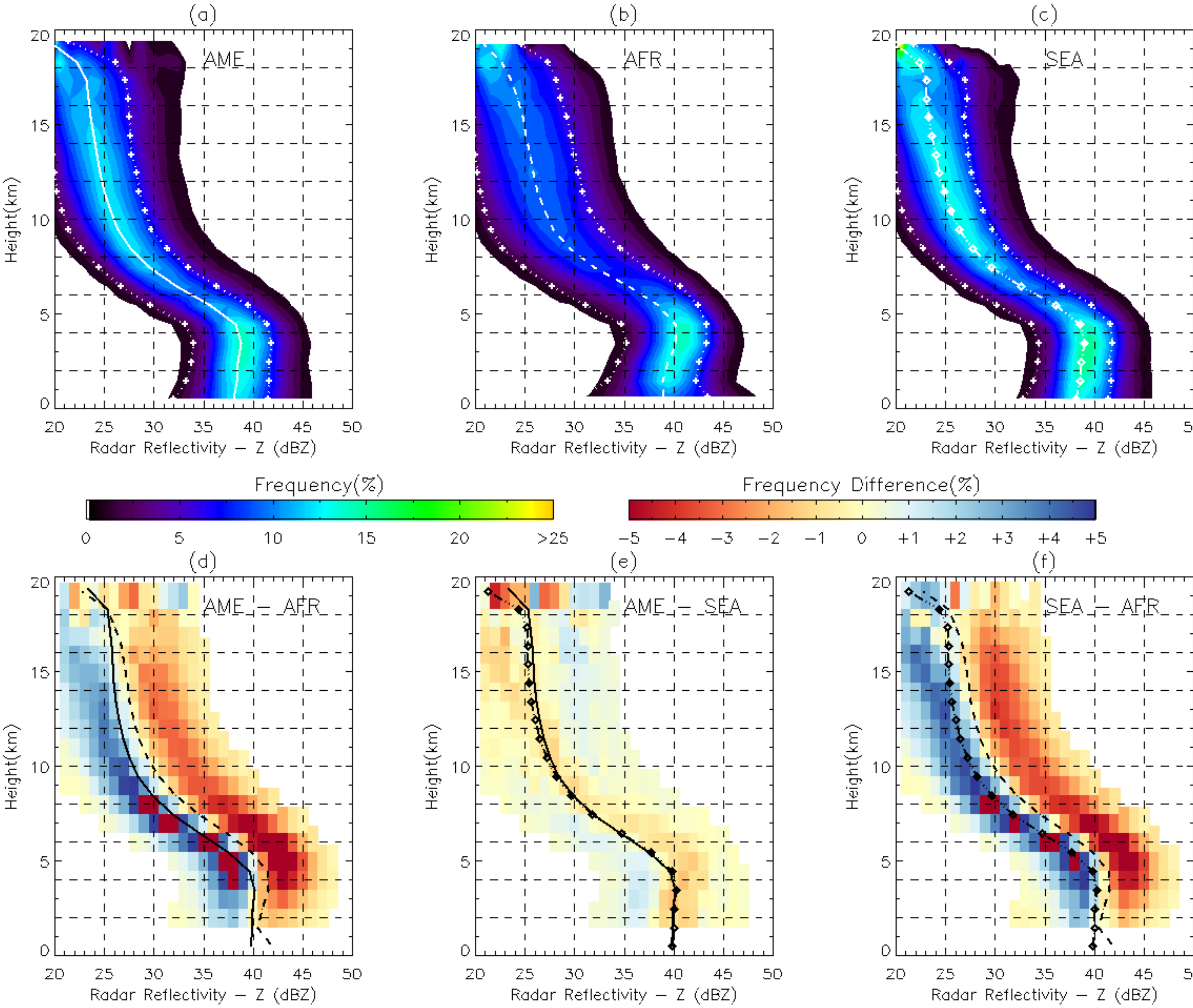

(a)
AME
(b)
AFR
(c)
SEA
Height(km)
Radar Reflectivity – Z (dBZ)
Frequency(%)
0
5
10
15
20
>25
Frequency Difference(%)
–5
–4
–3
–2
–1
0
+1
+2
+3
+4
+5
(d)
AME – AFR
(e)
AME – SEA
(f)
SEA – AFR

Figure 4.

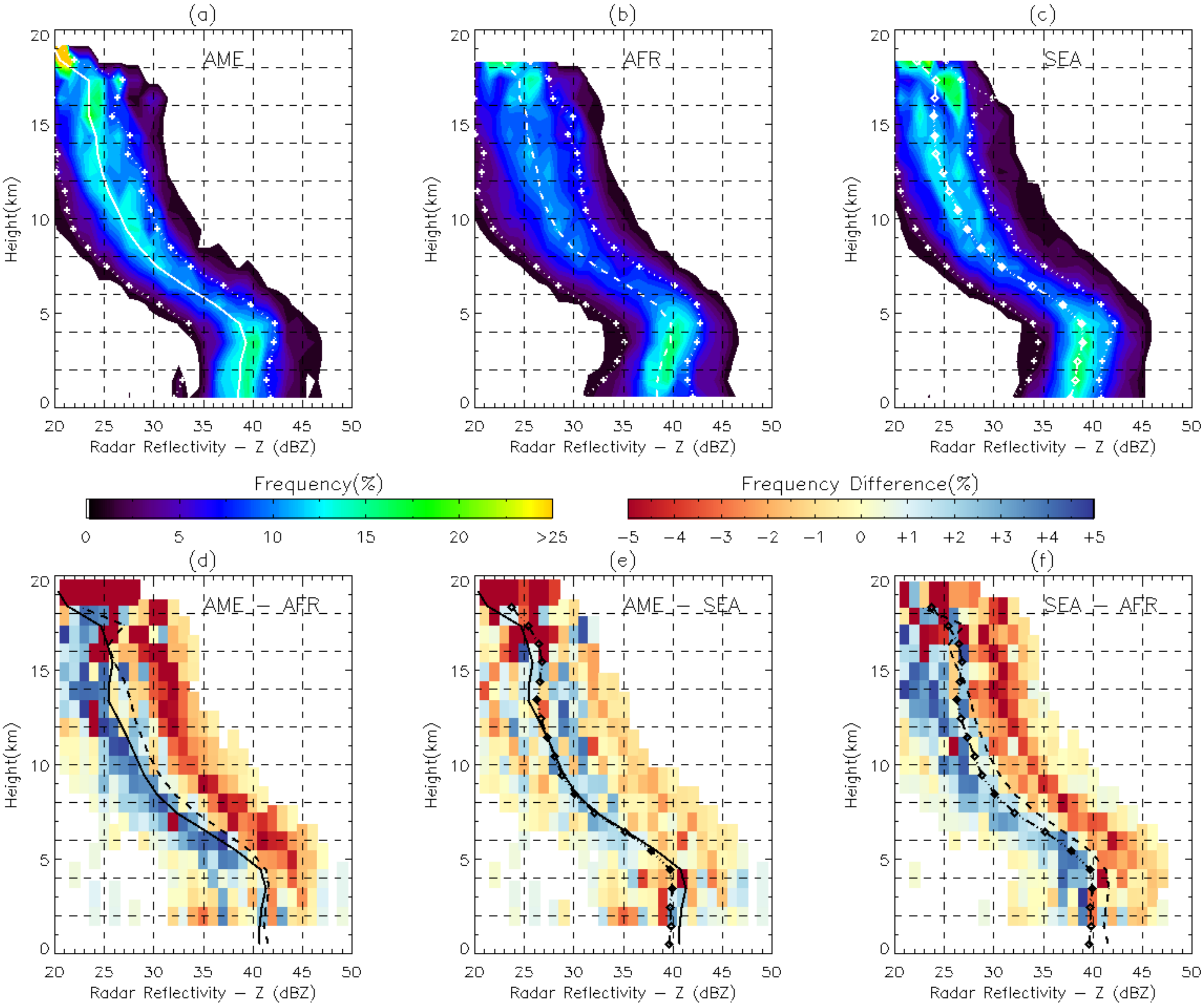
(a)
AME
(b)
AFR
(c)
SEA
Height(km)
Radar Reflectivity – Z (dBZ)
Frequency(%)
0
5
10
15
20
>25
Frequency Difference(%)
–5
–4
–3
–2
–1
0
+1
+2
+3
+4
+5
(d)
AME – AFR
(e)
AME – SEA
(f)
SEA – AFR

Figure 5.

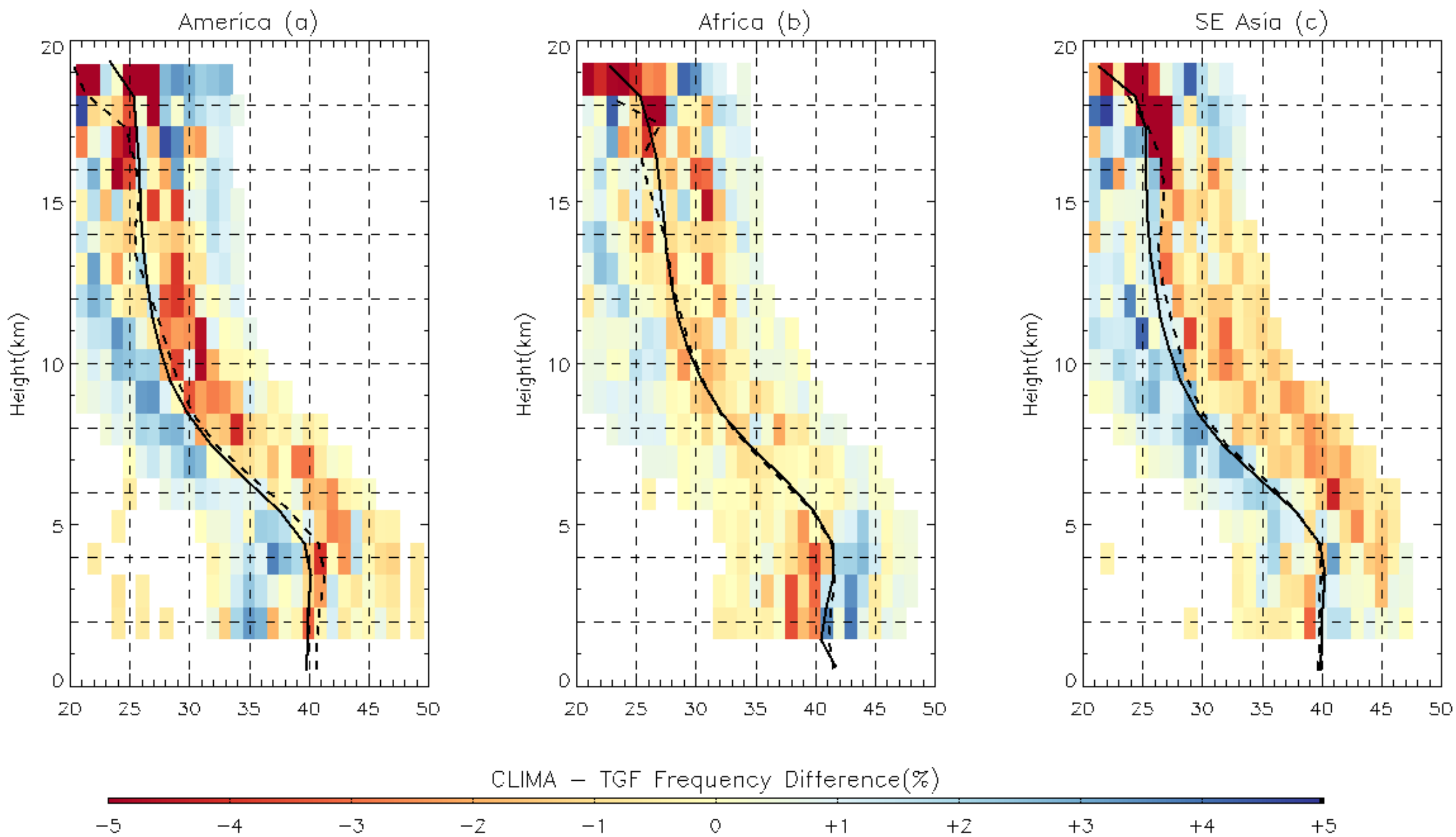
America (a)
Africa (b)
SE Asia (c)
Height(km)
0
5
10
15
20
20
25
30
35
40
45
50
CLIMA – TGF Frequency Difference(%)
−5
−4
−3
−2
−1
0
+1
+2
+3
+4
+5

Figure 6.

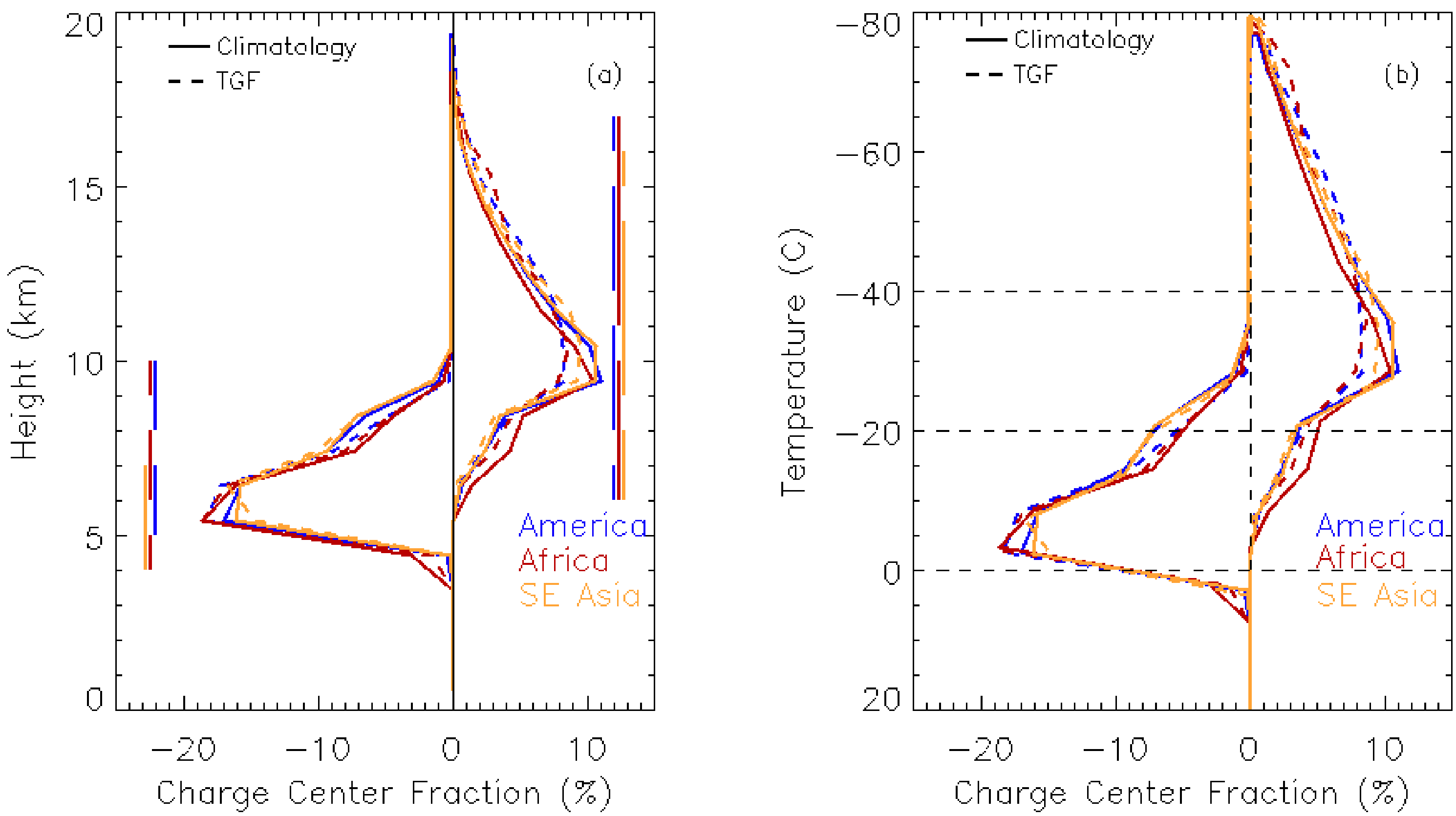

Climatology
TGF
(a)
Height (km)
Charge Center Fraction (%)
America
Africa
SE Asia
(b)
Temperature (C)
Charge Center Fraction (%)
America
Africa
SE Asia

Figure A1.

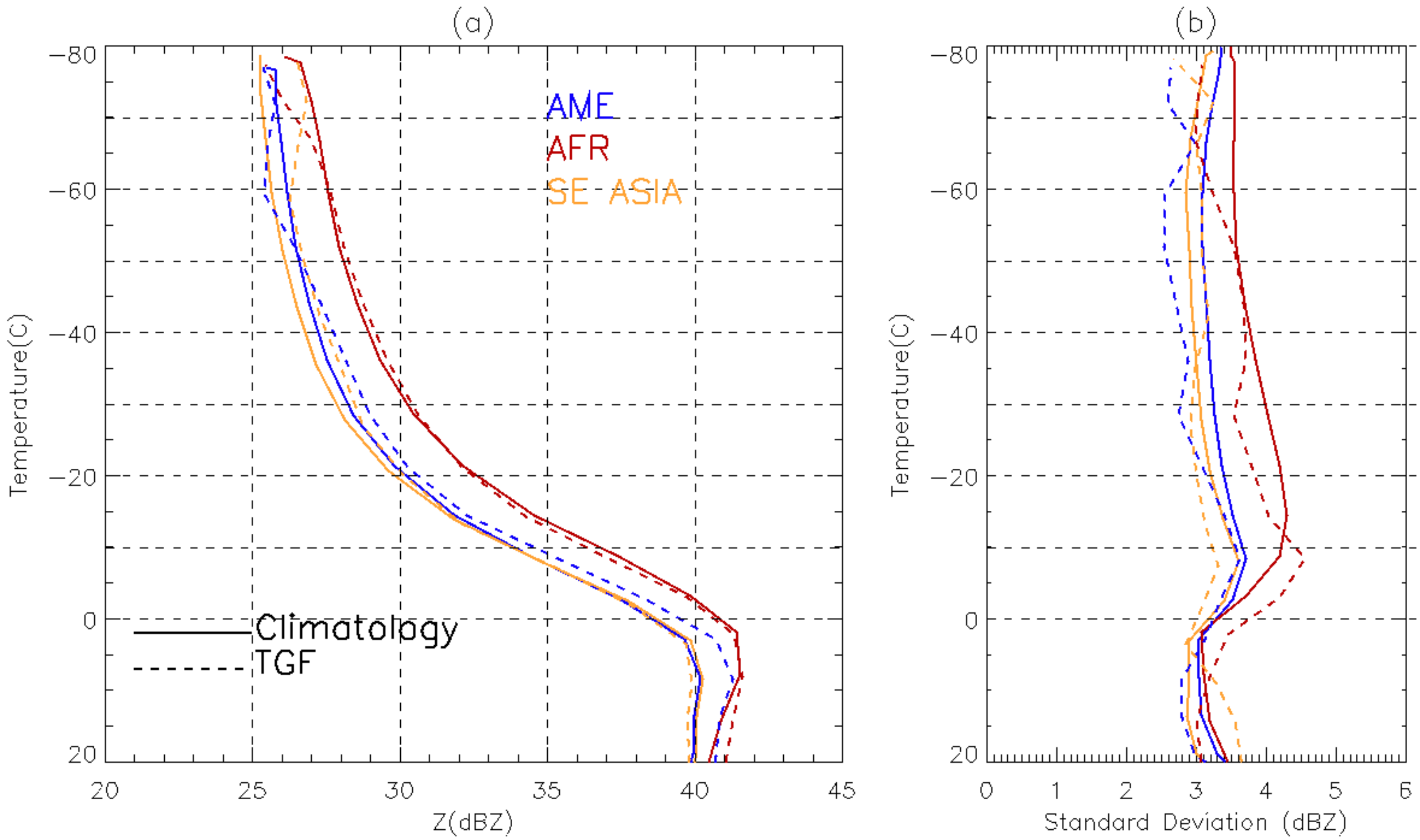

(a)
(b)
AME
AFR
SE ASIA
Climatology
TGF
Temperature(C)
Z(dBZ)
Standard Deviation (dBZ)

Figure B1.

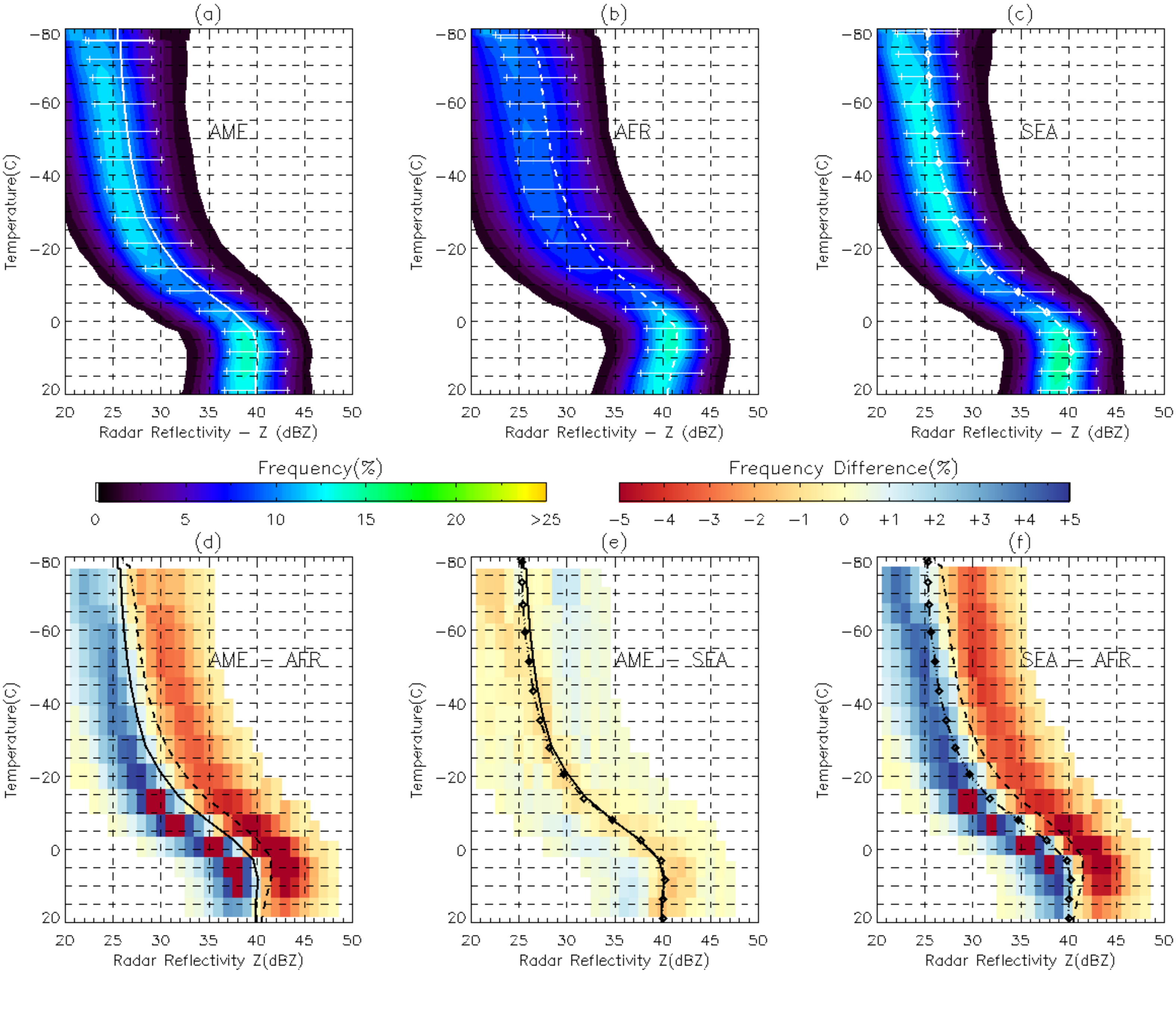

(a)
AME
(b)
AFR
(c)
SEA
Temperature(C)
Radar Reflectivity – Z (dBZ)
Frequency(%)
0
5
10
15
20
>25
Frequency Difference(%)
–5
–4
–3
–2
–1
0
+1
+2
+3
+4
+5
(d)
AME – AFR
(e)
AME – SEA
(f)
SEA – AFR
Radar Reflectivity Z(dBZ)

Figure B2.

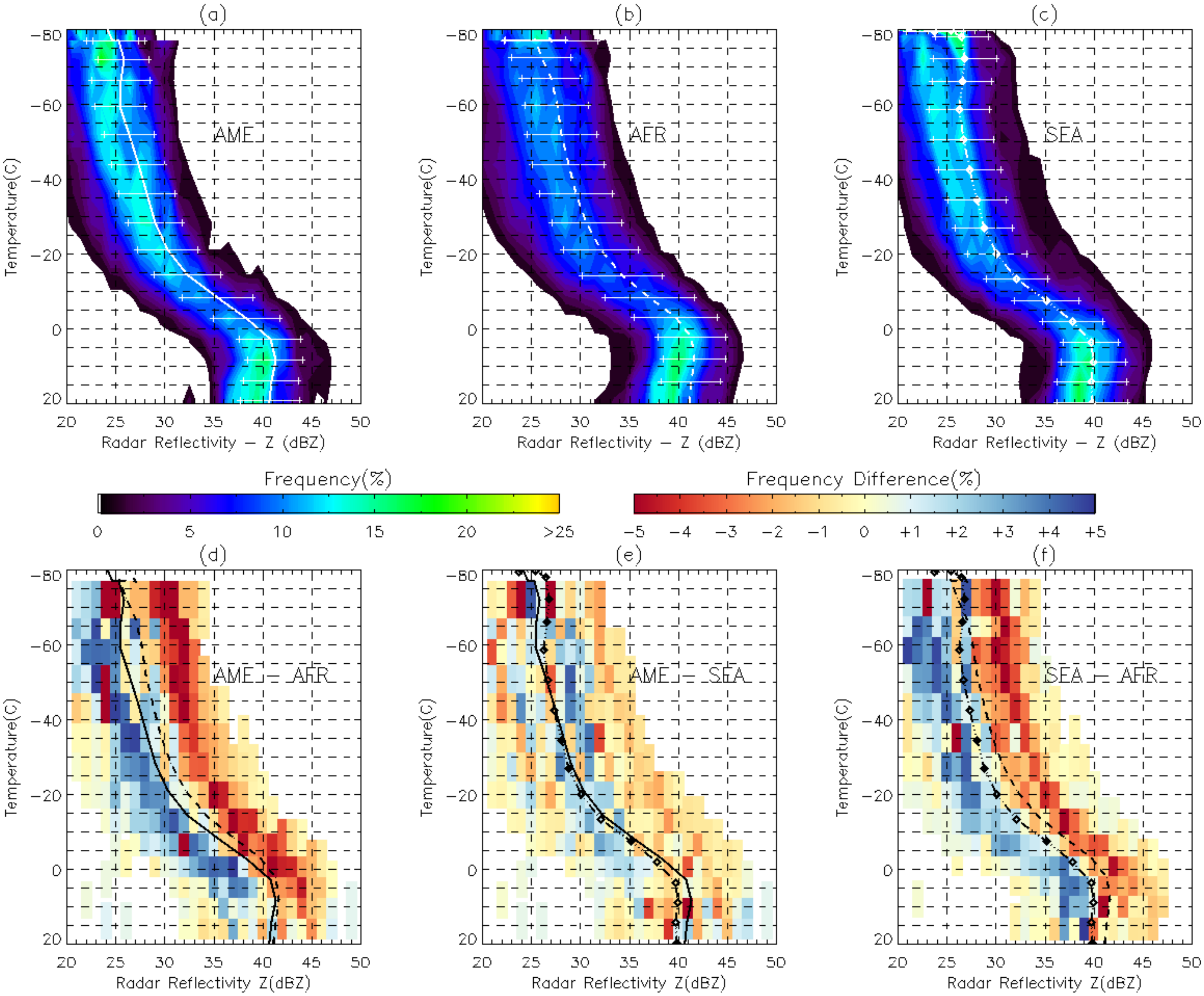
(a)
(b)
(c)
AME
AFR
SEA
Temperature(C)
Radar Reflectivity – Z (dBZ)
Frequency(%)
0
5
10
15
20
>25
Frequency Difference(%)
−5
−4
−3
−2
−1
0
+1
+2
+3
+4
+5
(d)
(e)
(f)
AME – AFR
AME – SEA
SEA – AFR
Radar Reflectivity Z(dBZ)

Figure B3.

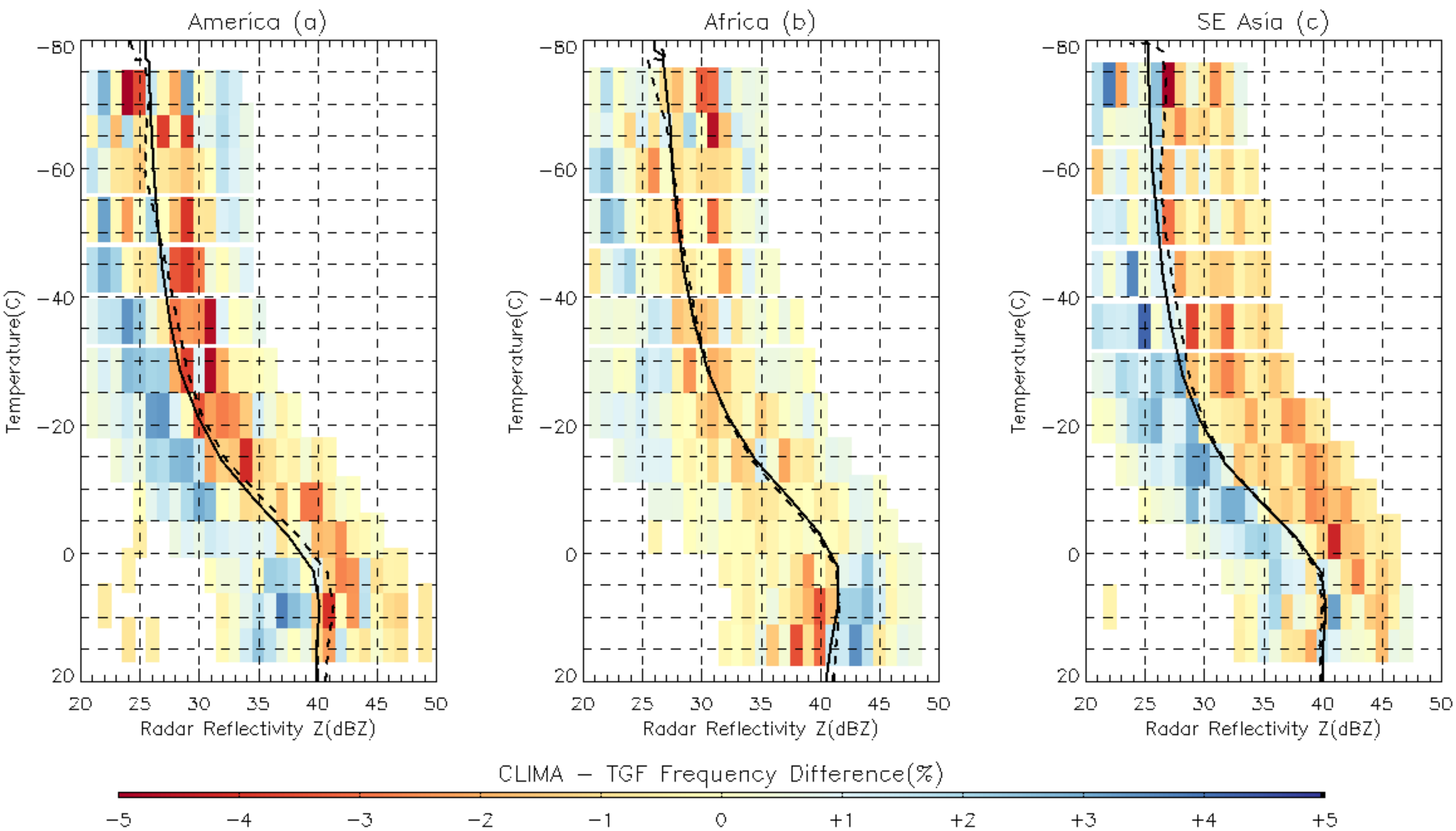

America (a)
Africa (b)
SE Asia (c)
Temperature(C)
-80
-60
-40
-20
0
20
20
25
30
35
40
45
50
Radar Reflectivity Z(dBZ)
CLIMA – TGF Frequency Difference(%)
-5
-4
-3
-2
-1
0
+1
+2
+3
+4
+5

Figure D1.

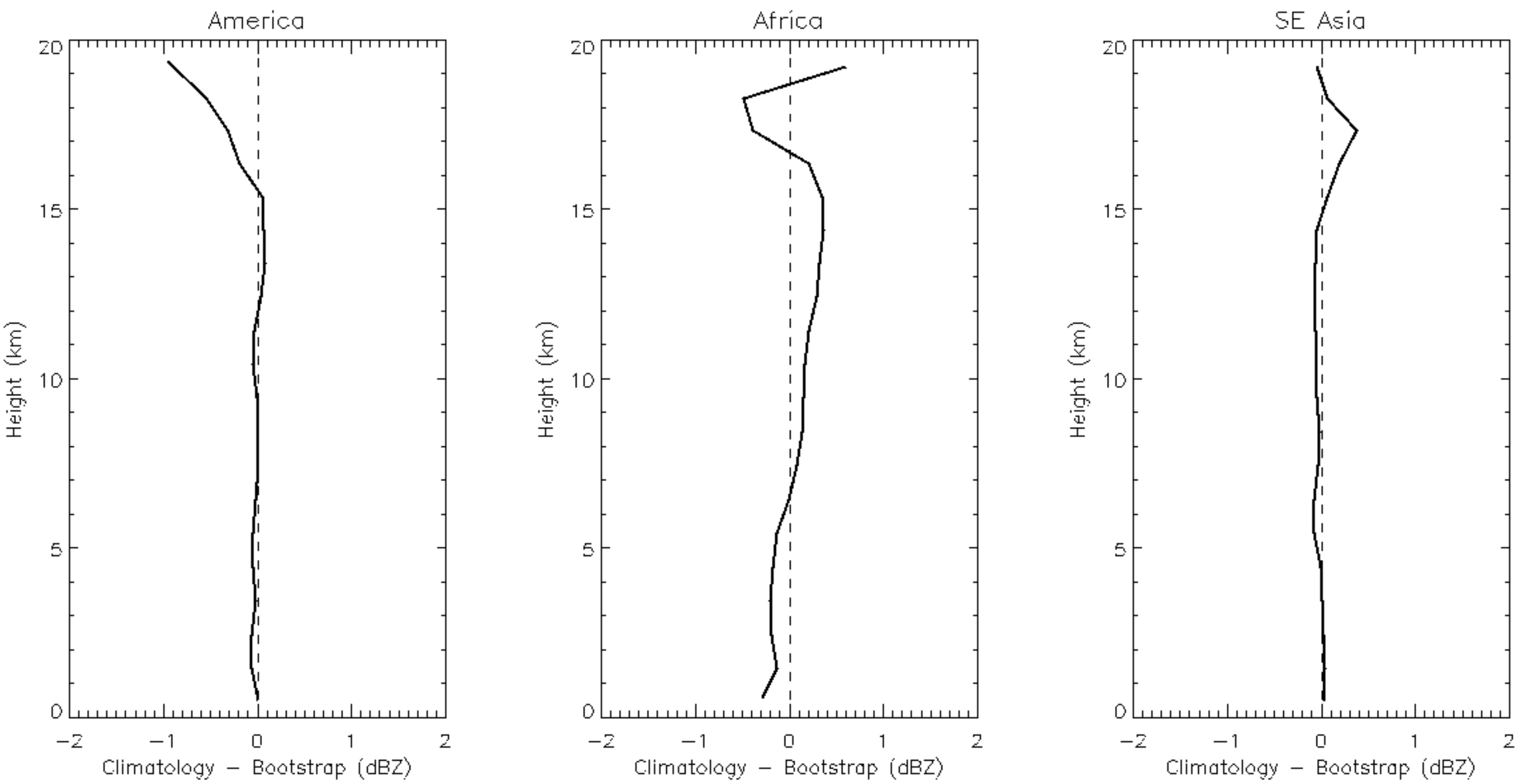
America
Africa
SE Asia
Height (km)
0
5
10
15
20
-2
-1
0
1
2
Climatology - Bootstrap (dBZ)

Figure D2.

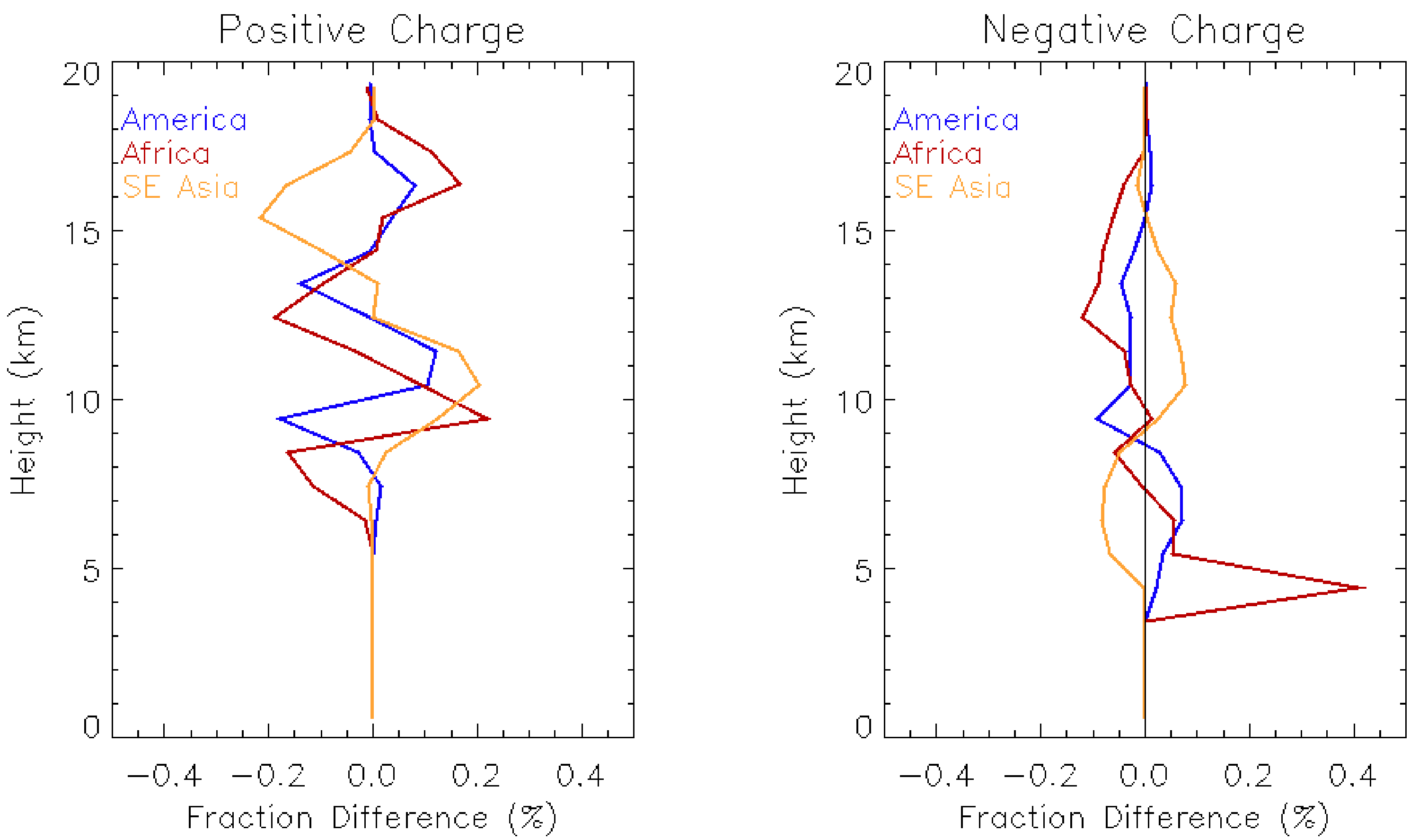

Positive Charge
Negative Charge
America
Africa
SE Asia
Height (km)
Fraction Difference (%)
0
5
10
15
20
−0.4
−0.2
0.0
0.2
0.4